Journal of Medicinal Chemistry

Article

N-(7-Cyano-6-(4-fluoro-3-(2-(3-(trifluoromethyl)phenyl)acetamido)phenoxy) benzo[d]thiazol-2-yl)cyclopropanecarboxamide (TAK-632) Analogues as Novel Necroptosis Inhibitors by Targeting Receptor-Interacting Protein Kinase 3 (RIPK3): Synthesis, Structure-Activity Relationships and In Vivo Efficacy

Hao Zhang, Lijuan Xu, Xia Qin, Xiaofei Chen, Hui Cong, Longmiao Hu, Long Chen, Zhenyuan Miao, Wannian Zhang, Zhenyu Cai, and Chunlin Zhuang

J. Med. Chem., **Just Accepted Manuscript** • DOI: 10.1021/acs.jmedchem.9b00611 • Publication Date (Web): 16 May 2019

N-(7-Cyano-6-(4-fluoro-3-(2-(3-(trifluoromethyl)phenyl)acetamido)phenoxy) benzo[d]thiazol-2-yl)cyclopropanecarboxamide (TAK-632) Analogues as Novel Necroptosis Inhibitors by Targeting Receptor-Interacting Protein Kinase 3 (RIPK3): Synthesis, Structure-Activity Relationships and In Vivo Efficacy

Hao Zhang,[1†] Lijuan Xu,[1†] Xia Qin,[3†] Xiaofei Chen,[2] Hui Cong,[1,2] Longmiao Hu,[3] Long Chen,[2] Zhenyuan Miao,[2] Wannian Zhang,[1,2*] Zhenyu Cai,[3, 4*] Chunlin Zhuang[1,2,5*]

[1] School of Pharmacy, Ningxia Medical University, 1160 Shengli Street, Yinchuan 750004, China

[2] School of Pharmacy, Second Military Medical University, 325 Guohe Road, Shanghai 200433, China

[3] National Center for Liver Cancer, Second Military Medical University, 225 Changhai Road, Shanghai 200438, China

[4] Cancer Institute, Fudan University Shanghai Cancer Center, Shanghai 200032, China

[5] Department of Chemistry, Fudan University, Shanghai 200433, China

ABSTRACT

Necroptosis, a form of programmed cell death, plays a critical role in various diseases, including inflammatory, infectious and degenerative diseases. We previously identified TAK-632 (**6**) as a potent inhibitor of necroptosis by targeting both RIPK1 and RIPK3 kinases. Herein, we performed three rounds of structural optimizations of TAK-632 and elucidated structure-activity relationships to generate more potent inhibitors by targeting RIPK3. The analogues with carbamide groups exhibited great anti-necroptotic activities and compound **42** showed >60-fold selectivity for RIPK3 than RIPK1. It blocked necrosome formation by specifically inhibiting the phosphorylation of RIPK3 in necroptotic cells. In a TNF-induced systemic inflammatory response syndrome model, it significantly protected mice from hypothermia and death at a dose of 5 mg/kg, which was much more effective than TAK-632. Moreover, it showed favorable and drug-like pharmacokinetic properties in rats with an oral bioavailability of 25.2%. Thus, these RIPK3-targeting small molecules represent promising lead structures for further development.

INTRODUCTION

Necroptosis is a caspase-independent, programmed necrosis.[1] It plays a critical role in various lethal diseases such as atherosclerosis, myocardial infarction, pancreatitis, ischemic brain damage, kidney damage, and systemic inflammatory response syndrome (SIRS).[2-9] Thus, targeting the pathologic necroptosis pathway has broad therapeutic relevance. Necroptosis can be induced by the activation of death receptors, such as TNF receptor 1 (TNFR1), CD95 (FAS), toll-like receptors 3/4 (TLR3/4), and interferons (IFNs).[10] Then, downstream receptor-interacting protein kinase 1 (RIPK1) interacts with RIPK3, initiating the formation of necrosomes and activating RIPK3 through phosphorylation.[11, 12] Subsequently, activated RIPK3 is recruited, and mixed lineage kinase domain-like protein (MLKL) is phosphorylated.[13, 14] Phosphorylated MLKL oligomerizes and then translocates into the plasma membrane to trigger membrane rupture, initiating necroptosis.[15-18] To date, RIPK1, RIPK3, and MLKL have been recognized as critical therapeutic targets in the machinery of necroptosis.[19]

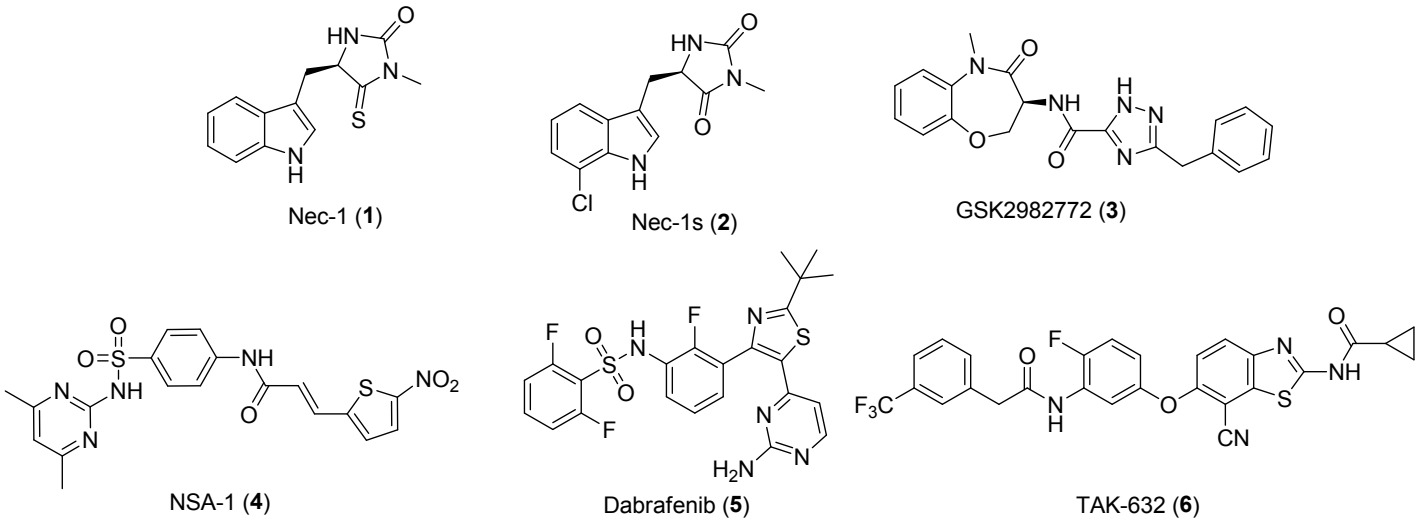

Figure 1. Representative known necroptosis inhibitors targeting RIPK1, RIPK3, or MLKL.

The first RIPK1 inhibitor, Nec-1 (**1**, Figure 1), was identified by the Yuan group in 2005.[6] However, its poor metabolic stability ($t_{1/2}$ < 5 min) limited further drug discovery efforts based on this compound. A subsequent analogue, Nec-1s (**2**), offered improved metabolic stability, but its potency remained moderate.[20-22] GlaxoSmithKline has made great advances in the discovery of necroptosis inhibitors. Compound **3** (GSK2982772), an RIPK1-specific inhibitor, has been advanced into phase II trials in patients with active

ulcerative colitis (UC) (NCT02903966), psoriasis (NCT02776033) or moderate to severe rheumatoid arthritis (NCT02858492).[23-26] A BBB permeable RIPK1 inhibitor, DNL747, with the chemical structure undisclosed, recently has been advanced into phase I trials in patients with amyotrophic lateral sclerosis (NCT03757351) and Alzheimer's disease (NCT03757325).[9, 27]

However, since RIPK3 can signal necroptosis independent of RIPK1, Nec-1 and these highly potent RIPK1 inhibitors cannot block RIPK3-independent necroptosis.[28] In addition, accumulating evidence suggests that RIPK1 is also involved in other signaling pathways independent of necroptosis such as apoptosis and inflammation.[29] Thus, identification of small molecules specifically targeting RIPK3 or MLKL is important for the development of new drug associated with this pathway. A few RIPK3 inhibitors, such as GSK'840, GSK'843, GSK'872 and GW'39B, have been reported.[30] However, these RIPK3 inhibitors have been shown to induce RIPK1-dependent apoptosis.[31, 32] Recently, dabrafenib (**5**), an FDA-approved drug for patients with $Braf^{V600E}$ melanoma, was identified as a RIPK3 kinase inhibitor to block necroptosis [33, 34] . However, so far no RIPK3 inhibitors have been used for clinical trials in necroptosis-associated diseases. In addition, although NSA-1 (**4**) is reported to be an MLKL inhibitor by covalent modification of the protein, it shows high cytotoxicity.[13, 35] Thus, identification of novel necroptosis inhibitors with lower cytotoxicity will undoubtedly has broad clinical relevance.[10]

Very recently, we identified the pan-Raf inhibitor TAK-632 (**6**) as novel necroptosis inhibitor by targeting both RIPK1 and RIPK3 kinases from an *in-house* library of fluorine-containing compounds.[36] In this study, we aimed to comprehensively analyze the structure-activity relationship (SAR) of TAK-632 and generate more potent analogues to inhibit necroptosis by targeting RIPK3.

RESULTS AND DISCUSSION

Chemistry.

Structural variations were introduced at three different positions of TAK-632. First, the amide-linked substituents at R^1 and R^2 were changed, but the cyano group (R^3) was left intact. Second, the cyano moiety was

removed, R^1 was fixed as a cyclopropyl group, and substituents on the phenylamide (R^2) were varied. Third, a carbamide was introduced at the R^2 position. All compounds in this study were prepared following the general strategies illustrated in Scheme 1 and Scheme 2. Key intermediates **m11-m16** were prepared following the procedure established in the literature.[37] Then, intermediates **m17-m22** were obtained by deprotection of the trifluoroacetyl group. Target compounds (**7-34**) were then obtained using HATU as the coupling reagent.

Scheme 1[a]

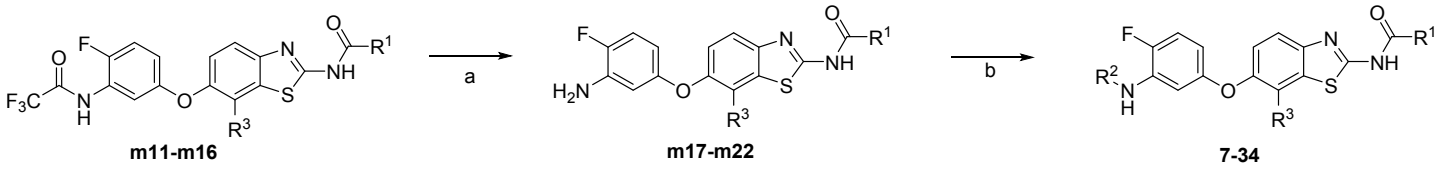

[a]Reagents and conditions: (a) $NaBH_4$, EtOH/MeOH (20:1), 0 °C to room temperature, 3 h, 95%-98%; (b) R^2COOH, HATU, dry pyridine, 85 °C, 8 h, 19%-71%. Details of the synthetic route and procedures for accessing intermediates **m11-m16** are presented in the Supporting Information.

Scheme 2[a]

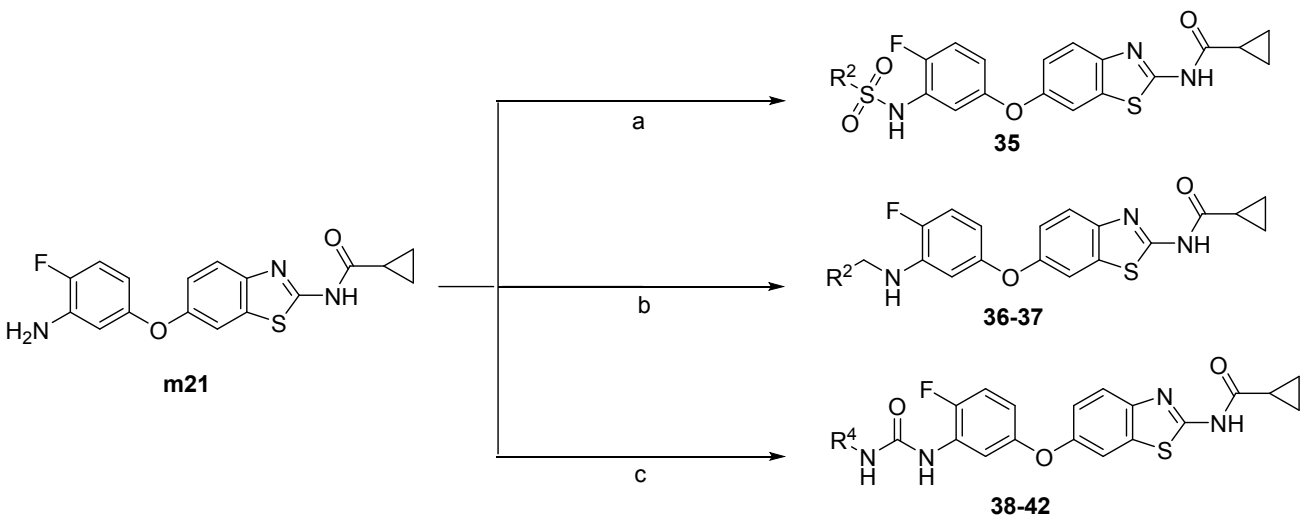

Reagents and conditions: (a) R^2SO_2Cl, dry pyridine, 0 °C to room temperature, 12 h, 45%; (b) R^2CHO, $NaBH_3CN$, AcOH, room temperature, 24 h, 26%-32%; (c) R^4NCO, DMF, MeCN or DMSO, room temperature, 12 h, 18%-54%.

The preparation of compounds **35-42** is shown in Scheme 2. Compounds **36** and **37** were obtained by reductive amination via treating intermediate **m21** with the appropriate benzaldehyde derivatives. Similarly, compound **35** was easily prepared by a substitution reaction. Compounds **38**-**42** were directly synthesized using different isocyanates. The procedures and characterization data of the key intermediates are presented in the Supporting Information. The final structures were fully characterized by ^{1}H NMR, ^{13}C NMR, and HRMS. All target compounds were purified to >95%, as determined by high-performance liquid chromatography (HPLC) analysis, prior to use in subsequent experiments.

Structure optimization, biological evaluation and SAR analysis identify necroptosis inhibitors by targeting RIPK3.

The anti-necroptosis activity of each compound was measured by a chemiluminescence assay using a model based on treating human HT-29 cells with TNF-α, Smac mimetic (SM-164) and a caspase inhibitor (z-VAD-FMK, abbreviated as TSZ).[36] The first round of optimizations was performed by modifying the substituents at R^1 and R^2 and retaining the cyano group (R^3) (Table 1). Initially, the cyclopropyl group of TAK-632 was replaced by ethyl (**7**), phenyl (**8**), nonyl (**9**) or benzyloxy (**10**) groups. The ability to inhibit TSZ-induced necroptosis at a concentration of 20 μM was completely lost; for comparison, parent compound TAK-632 exhibited an EC_{50} values of 1.44 ± 0.62 μM. Then, the cyclopropyl group was restored, and the substituents on the phenylamide (R^2) were changed. Compounds with *para*-nitrobenzyl (**11**), benzyl (**12**), *meta*-fluorobenzyl (**13**), and *meta*-trifluoromethylphenyl (**14**) groups, showed no inhibitory activities against necroptosis at 20 μM, indicating the importance of *meta*-trifluoromethyl group. At *ortho*-position of the benzyl moiety, an additional fluoro group was introduced to obtain compound **15**. It showed a similar activity (EC_{50} = 2.03±0.86 μM) with that of TAK-632. Thus, these results suggested a narrow window in which the structure of TAK-632 could be further modified.

Table 1. First round of optimization of TAK-632.

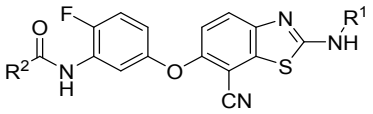

Compound	R^1	R^2	EC_{50}, (μM)[a]
7		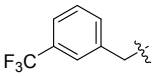	>20
8	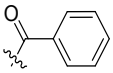	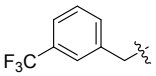	>20
9		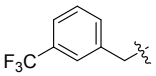	>20
10	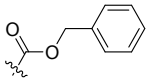	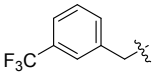	>20
11		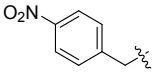	>20
12		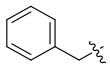	>20
13		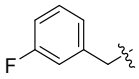	>20
14		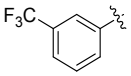	>20
15		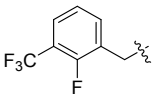	2.03±0.86
6 (TAK-632)		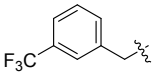	1.44±0.62

[a] Human HT-29 cells were pretreated with DMSO or the test compound and then stimulated with TNF-α (20 ng/mL), Smac mimetic (10 nM), and z-VAD-fmk (20 μM) (TSZ) for 16 h. The inhibition of TSZ-induced necroptosis in HT-29 cells is presented as the EC_{50} ± SD. All experiments were repeated independently at least 3 times.

TAK-632 is a pan-Raf inhibitor;[38] however, Raf kinase is not involved in the necroptosis signaling pathway.[33] In a previous study, we experimentally showed that TAK-632 protects cells from necroptosis by targeting RIPK1 (K_d = 480 nM) and RIPK3 (K_d = 105 nM).[36] Thus, a structural optimization study was performed to improve the anti-necroptotic activity and the inhibition of RIPK1 and/or RIPK3. The first potential position for structural optimization was the cyano group of TAK-632, which may slightly improve Raf kinase inhibition but it is not critical to the activity.[37] To our delight, compound **16**, lacking the cyano group, exhibited approximately 8-fold better anti-necroptotic activity, ~4-fold and ~2-fold better *in vitro* RIPK1/3 kinase inhibition (Table 2) and ~2-fold lower inhibition of Raf kinase.[36] However, it showed slight cytotoxicity with a CC_{50} value of 36.50 μM. Encouraged by this cyano-free analogue of TAK-632, we then used **16** as a lead compound for further optimization. The *meta*-trifluoromethyl group on the benzylamine of **16** was critical to the anti-necroptotic activity. Compound **17**, with an *ortho*-trifluoromethyl group, had an EC_{50} value of 11.35 μM, which is a ~66-fold decrease relative to that of **16**. Introducing an additional fluorine atom at the *ortho*- (**18**) or *para*-position (**19**) resulted in a ~3-fold lower effects on necroptosis and RIPK1/3 kinase activity. However, a chlorine atom at the *ortho*-position (**20**) completely eliminated the activity. An additional trifluoromethyl group (**21**) in the *meta*-position was detrimental to the anti-necroptotic activity (EC_{50} = 9.7 μM). The presence of two adjacent methyl groups (**22**) decreased the anti-necroptotic effect to 1.67±0.83 μM and the RIPK1 kinase activity to 1.2 μM, while the RIPK3 kinase activity (K_d = 72 nM) was similar to that of **16**. However, more active compounds (**18**, **19** and **22**) showed unfavorable RIPK1 binding, suggesting small substituents on the phenyl ring are tolerated and can preserve RIPK3 inhibition ability.

Then, we focused on mono-substituted benzylamines to improve the anti-necroptotic potency. The nitro- (**23**), methyl- (**24**), and methoxyl- (**25**) substituted analogues showed anti-necroptotic potencies that were 2~4-fold better than that of TAK-632, and they had cell potencies and kinase inhibitory activities similar to those of **16**. Compounds **24** and **25** had better RIPK3 inhibitory activities (K_d = 33 and 55 nM) than **16**. Introducing a trifluoromethoxyl group (**26**) resulted in the best anti-necroptosis potency seen in this series (EC_{50} = 60±30 nM). In addition, this compound showed increased the inhibitory activity for RIPK1 while retaining the inhibitory activity for RIPK3. Replacing the trifluoromethyl group of **16** with a hydroxyl group (**27**) completely

removed the activity, and the installation of a cyano group (**28**) was also detrimental to its inhibitory potency, resulting in an EC_{50} value of 1.29±0.47 μM. The RIPK1 inhibitory activity of compound **28** was 8-fold lower and its RIPK3 inhibitory ability was comparable to that of compound **16**. Then, the phenyl ring was replaced by a pyridinyl group (**29**), and the resulting compound possessed an EC_{50} of 0.32±0.05 μM against cell necroptosis. However, removing the trifluoromethyl group from compound **29** to give **30** was detrimental to the activity, which decreased to 8.3 μM. Introducing heterocycles (**31** and **32**) negatively impacted cell necroptosis activity, and **31** and **32** showed 10~20-fold lower activities than **16**. Nevertheless, the selectivity for RIPK3 over RIPK1 was maintained. The binding affinity of compound **31** for RIPK3 was K_d = 81 nM, and its affinity for RIPK1 was 13-fold lower. Indolyl analogue **32** had K_d values of 4.8 and 1.4 μM for RIPK1 and RIPK3, respectively. Moreover, it is also reported that the linker in lead molecules might be useful to the selectivity.[39] Therefore, an additional methylene (**33**) unit was added in the linker between the trifluoromethylphenyl and amide moieties, but this decreased the anti-necroptotic activity approximately 4-fold compared with that of **16**; however, the activity of **33** was 2-fold higher than that of TAK-632. Introducing cyclopropyl (**34**) or sulfamide (**35**) moieties as the linker destroyed the activity. When the carbonyl of the amide was removed to afford benzyl-substituted compounds **36** and **37**, the resulting necroptosis inhibitory activities were undetectable at 20 μM. These results suggest the importance of the amide linker for further optimization. Moreover, the cytotoxicities of these analogues that showed anti-necroptotic activities were significantly lower (CC_{50} > 50 μM).

Table 2. Second round of optimization of TAK-632.

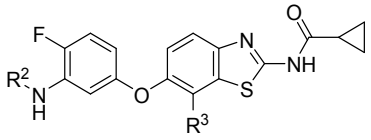

Compound	R^2	R^3	EC_{50}, (μM)[a]	Cytotoxicity (CC_{50}, μM)	RIPK1 (K_d, nM)[b]	RIPK3 (K_d, nM)

16[c]	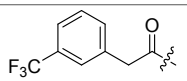	H	0.17±0.03	36.50	97	77
17	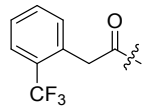	H	11.35	N.D.	N.D. [d]	N.D.
18	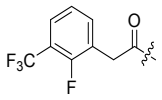	H	0.49±0.07	>50	510	99
19	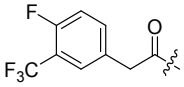	H	0.40±0.04	>50	590	130
20	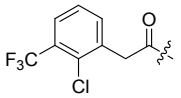	H	>20	N.D.	N.D.	N.D.
21	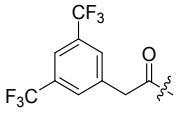	H	9.7	>50	N.D.	N.D.
22	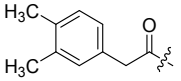	H	1.67±0.83	>50	1200	72
23	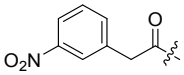	H	0.61±0.05	>50	770	110
24	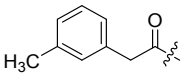	H	0.38±0.05	>50	320	33
25	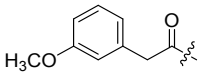	H	0.33±0.05	>50	240	55
26	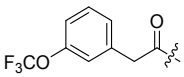	H	0.06±0.03	>50	49	120
27	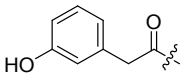	H	>20	N.D.	N.D.	N.D.

28	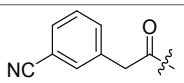	H	1.29±0.47	>50	780	120
29	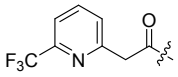	H	0.32±0.05	>50	220	280
30	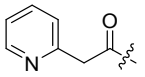	H	8.3	N.D.	N.D.	N.D.
31	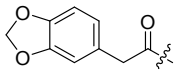	H	2.32±0.94	>50	1100	81
32	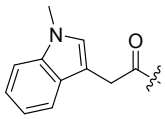	H	3.81±0.92	>50	4800	1400
33[c]	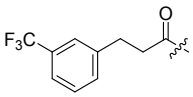	H	0.65±0.11	>50	510	790
34[c]	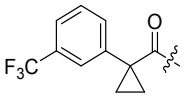	H	>20	>50	N.D.	N.D.
35[c]	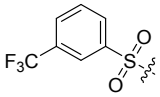	H	>20	N.D.	N.D.	N.D.
36	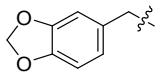	H	>20	N.D.	N.D.	N.D.
37[c]	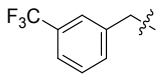	H	>20	N.D.	N.D.	N.D.
6 (TAK-632)	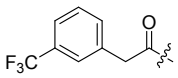	CN	1.44±0.62	>50	480	105

[a] Inhibition of TSZ-induced necroptosis in HT-29 cells.

[b] The inhibitory effects of the compounds on RIPK1 and RIPK3 kinases were detected by a KINOMEscan™ assay. The experiments were conducted in duplicate, and the K_d values are presented as the average.

[c] These compounds have been included in our previous publication.[36]

[d] N.D. = not determined if the anti-necroptotic activity was higher than 5 μM.

Next, the third round of optimization focused on the substituents on the amide fragment in order to improve the selectivity. We first introduced a carbamide group into compound **16**, which is a potential functional group for kinase binding with additional hydrogen bond. To our delight, this series of compounds showed great selectivity for RIPK3 over RIPK1; their selectivities were much higher than those of TAK-632 (selectivity = 4.6) and **16** (no selectivity). Then, different substituents were introduced at the *meta*-position due to the substantial influence of groups at this position on the anti-necroptotic activity. The methoxyl (**38**) and methyl (**39**) analogues showed anti-necroptosis EC_{50} values of 1.37±0.08 and 0.58±0.16 μM, respectively. They possessed binding affinities for RIPK3 with K_d values of 69 and 93 nM and for RIPK1 with K_d values of 3.6 and 2.2 μM, respectively. Compound **40**, with an ethoxycarbonyl group, showed an RIPK3/1 selectivity of >69.4; however, its EC_{50} value was 7.74±1.87 μM, making it less potent than TAK-632. Compound **41**, with an acetyl group, exhibited the best RIPK3 binding affinity (K_d = 53 nM) and the highest RIPK3/1 selectivity (> 94.3). Moreover, its anti-necroptotic activity was 7-fold higher than that of compound **40**. Bromo-substituted compound **42** had a K_d value of 81 nM toward RIPK3 and no binding for RIPK1 at 5 μM (selectivity > 61.7). **42** also exhibited good anti-necroptotic activity with an EC_{50} value of 0.44±0.10 μM, which is comparable to that of **16**, and low cytotoxicity (CC_{50} > 50 μM).

Table 3. Structural optimization of compound **16**.

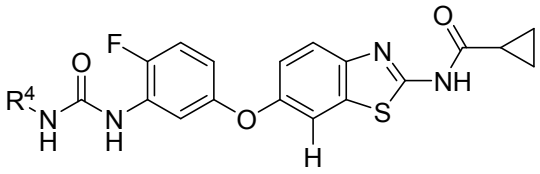

Compound	R^4	X	EC_{50}, (μM)[a]	Cytotoxicity (CC_{50}, μM)	RIPK1 (K_d, nM)[b]	RIPK3 (K_d, nM)	Selectivity RIPK3/1

38	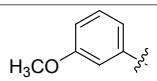	O	1.37±0.08	>50	3600	69	52.1
39	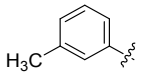	O	0.58±0.16	>50	2200	93	23.6
40	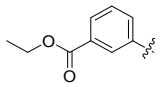	O	7.74±1.87	>50	>5000	72	>69.4
41	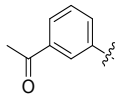	O	1.0±0.28	>50	>5000	53	>94.3
42	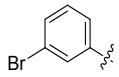	O	0.44±0.10	>50	>5000	81	>61.7
6 (TAK-632)	/	/	1.44±0.62	>50	480	105	4.6

[a] Inhibition of TSZ-induced necroptosis in HT-29 cells.

[b] The inhibitory effects of the test compounds on RIPK1 and RIPK3 kinases were detected by a KINOMEscan™ assay. The experiments were conducted in duplicate, and the K_d values are presented as the average.

With the above structural and biological information, SARs can be derived for further structural optimization (Figure 2). (1) A narrow SAR of TAK-632 analogues with cyano groups is observed. (2) The removal of the cyano group has a positive effect on the anti-necroptotic activity. (3) Small substituents at the *para*- and *ortho*-positions are tolerated. The linker between the trifluoromethylphenyl and amide moieties is of great importance to the anti-necroptotic activity. (4) The carbamide group has a positive effect on the anti-necroptosis activity and the selectivity for binding RIPK3 over RIPK1.

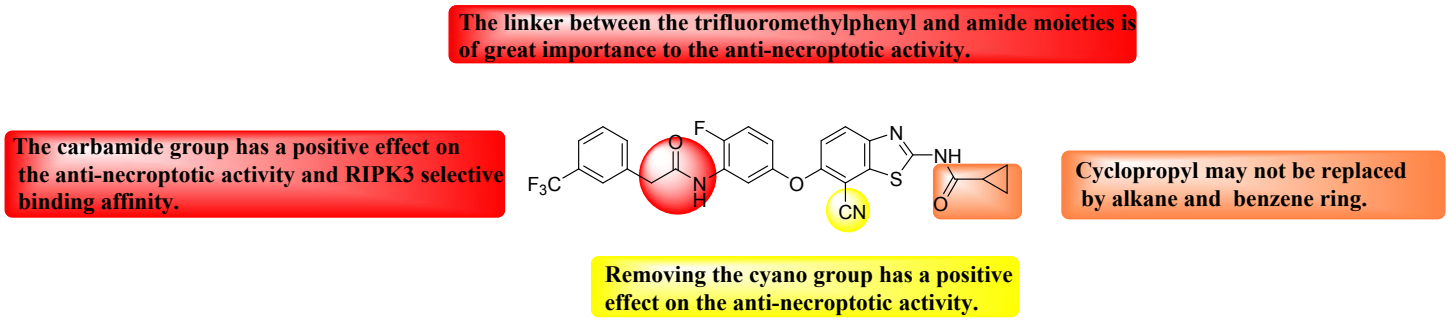

Figure 2. Systematic summary of the SAR.

Kinase Inhibitory Profiles of Compound 42 and Molecular Docking Analysis.

In our screen, we found that compound **26** showed the highest anti-necroptotic activity in HT-29 cells by inhibiting the kinase activities of both RIPK1 and RIPK3. The dual RIPK1 and RIPK3 kinase inhibitors may have off-target effects since RIPK1 is also involved in other signaling pathways independent of necroptosis such as apoptosis and inflammation.[29] In this study, we aimed to comprehensively analyze the structure-activity relationship (SAR) of TAK-632 and generate more potent analogues to inhibit necroptosis by targeting RIPK3. Thus, we selected compound **42**, a compound with imporved anti-necroptotic activity by specifically targeting RIPK3, for further evaluation.

The kinase inhibitory profile against 25 different kinases including Raf family kinases was performed based on the previous study[37] (Table 4). Similar to TAK-632 and compound **16**,[36] compound **42** targeted additional 6 kinases other than RIPK3 *in vitro* (% Ctrl < 10). In cells, the anti-necroptotic activity of compound **42** cannot be explained by these additional targets since vemurafenib (a Raf inhibitor) and vandetanib (a VEGFR2 inhibitor) with similar target profiles did not inhibit necroptosis.[33, 40] Besides, the identified targets of compound **42**, including Raf, VEGFR, PDGFR and SRC, were not involved in necroptotic signaling pathway.[33, 41]

Table 4. Kinase selectivity of compound **42**

Kinase	**%Ctrl @ 1000 nM**	**Kinase**	**%Ctrl @ 1000 nM**	**Kinase**	**%Ctrl @ 1000 nM (K_d, nM)**
Braf (wt)	3.6	CDK2	93	JNK1	79

Braf (V600E)	1.8	CDK3	96	p38α	23
EGFR	33	CDK7	81	IKKα	100
EGFR (L858R)	61	GSK3B	100	IKKβ	97
ERK1	100	MAP3K4	100	PDGFRA	5.3
FGFR2	22	MAPKAPK2	100	PDGFRB	0
FGFR3	62	MEK1	100	SRC	0
Raf1	13	MEK2	83	MET	14
VEGFR2	2.8				

[a] The inhibitory effects were detected by a KINOMEscan™ assay and reported as %Ctrl (DMSO = 100% Ctrl)

The molecular docking studies were performed in order to understand the structural basis of the protein target specificity. Two compounds (**16** and **42**) biochemically targets RIPK1 and/or RIPK3 were selected. Compound **16** could bind well with RIPK1 (Figure 3A) and RIPK3 (Figure 3C). Compound **42** could bind well with RIPK3 (Figure 3D) but not RIPK1 (Figure 3B). A key hydrogen-bonding interaction between the thiazole ring and protein residue D156 was observed in the predicted model of compound **16**-RIPK1 complex. Besides, the benzothiazole of **16** formed strong π-π stacking interactions with F162. The aniline group was located in the gatekeeper region (I43, K45 and M92 residues) and the trifluorophenyl group was inserted through the gatekeeper pointing to the solvent exposed region. However, in the predicted model of **42**-RIPK1 complex, the key hydrogen bond with D156 was missed as the benzothiazole ring was flipped (Figure 3B and Figure 3E). Although the compound showed a similar conformation as compound **16**, the repulsion of carbamide group and amide group of K45 made **42** slightly moved (Figure 3E). These might disrupt its interaction with RIPK1 and probably made **42** inactive toward RIPK1. For RIPK3, we generated a homology model of human RIPK3 based on murine RIPK3 (PDB entry: 4M69), which shares 69% sequence identity and 77% sequence similarity with each other.[42] Both **16** and **42** showed similar binding conformations in a "U" mode with RIPK3 (Figure 3F), and a key hydrogen bond between the nitrogen of thiazole ring and T94 was observed. The trifluorophenyl or bromophenyl group was inserted into the region of G31, D142 and N147. Besides, the carbamide formed

additional hydrogen bonds with S146 and a halogen bond was formed by the bromo group with G31 and N147, which were probably useful to maintain the "U" conformation and kinase inhibitory activity.

As compound **42** also inhibited the kinase activity of B-raf, the binding mode of compound **42** with B-raf kinase was predicted (Figure S1). Compound **42** showed similar binding conformation with TAK-632 and kept all the key interactions of TAK-632 with B-raf, including three hydrogen-bonding interactions with D593, E500 and C531, π-π stacking interactions with W530 and F594, and π-catin interaction with K482. Additionally, **42** formed a hydrogen-bonding interaction with E500 as the introduction of carbamide group. In future, it would be of importance to generate more derivatives of TAK-632 to segregate the specificity for RIPK3 from its other targets. Collectively, the molecular docking analysis further support the experimental results that compound **42** targets RIPK3 but not RIPK1.

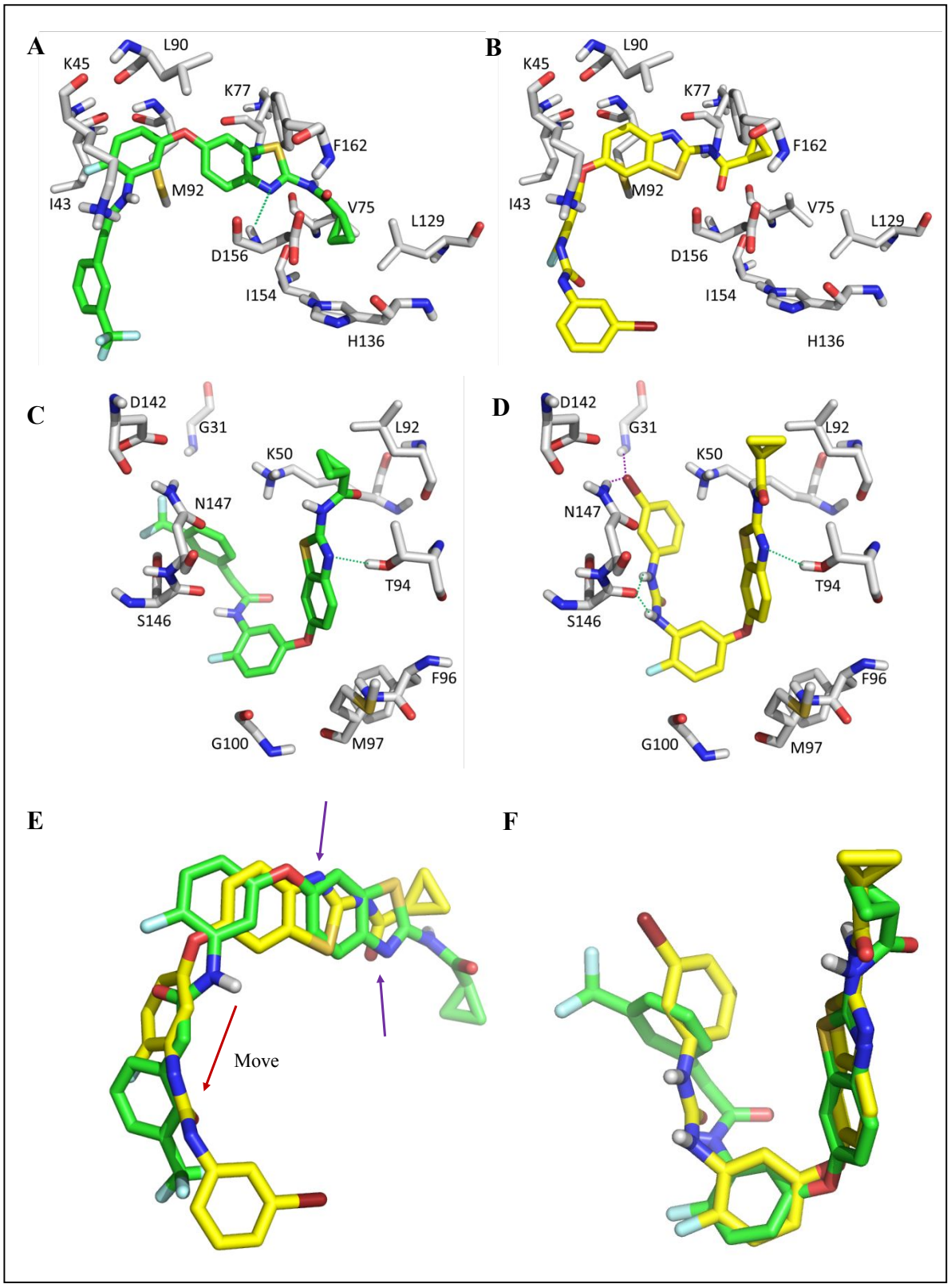

Figure 3. Binding modes of compound **16** (carbon in green) or **42** (carbon in yellow) with RIPK1 (PDB entry: 6HHO) and RIPK3 (A homology model based on PDB 4M66). (A) compound **16** with RIPK1; (B) compound **42** with RIPK1; (C) compound **16** with RIPK3; (D) compound **42** with RIPK3. Superposition of the binding modes of compound **16** (carbon in green) or **42** (carbon in yellow) with RIPK1 or RIPK3. (E) compounds **16**

and **42** with RIPK1. (F) compounds **16** and **42** with RIPK3. Residues of enzymes are depicted as grey sticks. Hydrogen bonds and halogen bonds are depicted as green and purple dash lines.

Compound 42 specifically inhibits necroptosis.

As compound **42** has been shown to inhibit the kinase activity of RIPK3 *in vitro*, we then further evaluate its anti-necroptotic ability in cells. It also protected against TNF-α, cycloheximide and z-VAD-FMK (TCZ)-induced necroptosis in human HT-29 cells (Figure 4A), but it did not protected cells from TS- or TC-induced apoptosis (Figure 4B). In murine L929 cells, we found that compound **42** protected against necroptosis induced by TNF-α and z-VAD-fmk (TZ) in a dose-dependent manner (Figure 4C). The above results indicate that compound **42** specifically inhibits the necroptosis pathway.

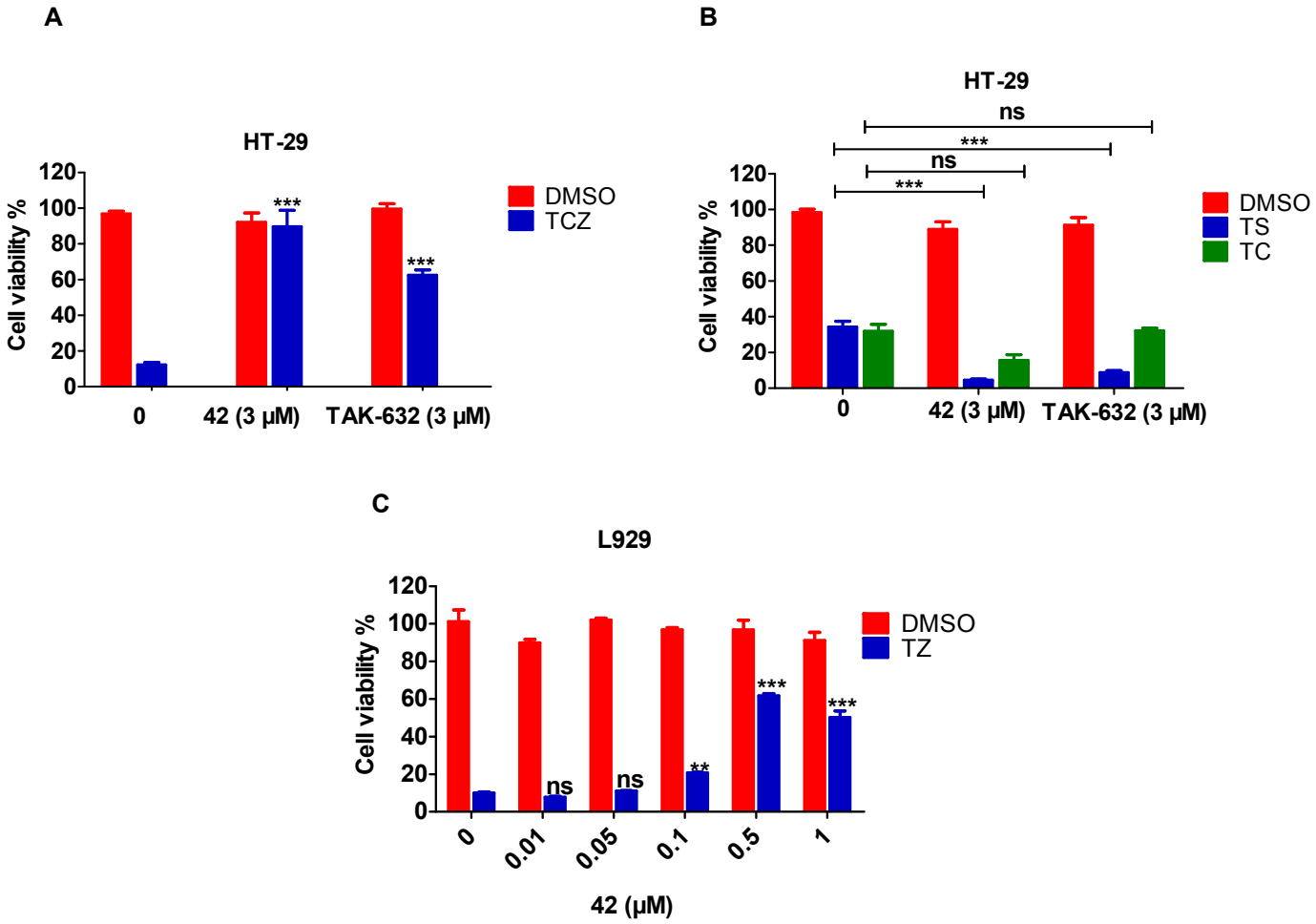

Figure 4. Effects of TAK-632 analogues on necroptosis and apoptosis. (A) The HT-29 cells were pretreated with DMSO, compound **42** (3 μM) or TAK-632 (3 μM), and then stimulated with TNF-α (20 ng/mL), cycloheximide (5 μg/mL) and z-VAD-fmk (20 μM) (TCZ) for 12 h. (B) The HT-29 cells were pretreated with DMSO, compound **42** or TAK-632 (3 μM), and then stimulated with TNF-α (20 ng/mL) plus cycloheximide (5 μg/mL) (TC) or TNF-α (20 ng/mL) plus Smac mimetic (10 nM) (TS) for 20 h. (C) The L929 cells were pretreated with DMSO or compound **42** at the indicated concentrations and then stimulated with mouse TNF-α (20 ng/mL) and z-VAD-fmk (20 μM) (TZ) for 4 h. **p < 0.005, ***p < 0.0005, compounds **42** or TAK632 versus no treatment.

Compound 42 blocks necrosome formation by inhibiting the phosphorylation of RIPK3.

To investigate the inhibitory mechanism of compound **42** against necroptosis, we examined phosphorylation of RIPK1, RIPK3, and MLKL in TSZ-treated HT-29 cells with or without compound **42**. Consistent with the *in vitro* kinase assay, compound **42** did not influence the phosphorylation of RIPK1 (Figure 5A). However, it selectively inhibited the phosphorylation of RIPK3 and MLKL. Since the phosphorylation of RIPK1 and RIPK3 are required for RIPK1-RIPK3 necrosome formation,[12] we then explored the formation of necrosome in HT-29 cells after pretreated with compound **42** and we found that compound **42** blocked TSZ-induced necrosome formation (Figure 5B). Thus, compound **42** blocks necrosome formation by inhibiting TSZ-induced phosphorylation of RIPK3.

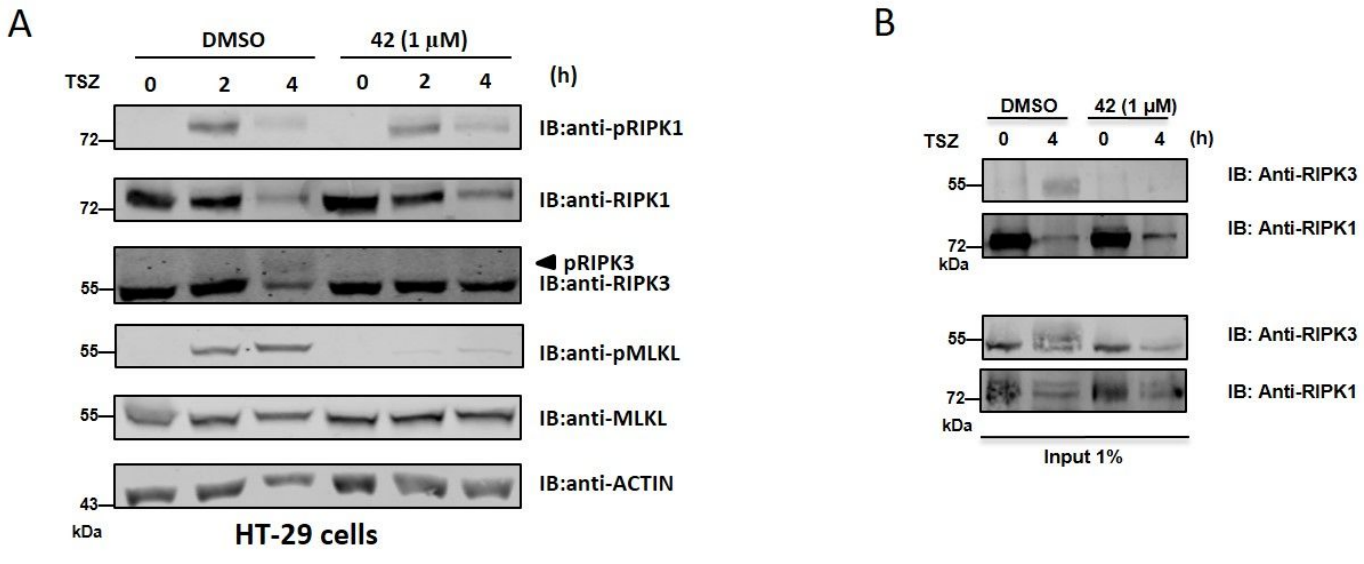

Figure 5. Compound **42** blocks necrosome formation by inhibiting the phosphorylation of RIPK3. (A) The HT-29 cells were pretreated with compound **42** (1 μM) and then stimulated with TSZ at the indicated time points. The cells were lysed and immunoblotted with the indicated antibodies. (B) The HT-29 cells were treated with DMSO or compound **42** (1 μM) for 4 h. The cell lysates were immunoprecipitated with an anti-RIPK1 antibody (IP: RIPK1) and analyzed by immunoblotting with the indicated antibodies.

Compound 42 protects mice from TNF-induced systemic inflammatory response syndrome (SIRS).

To explore whether compound **42** protects against RIPK-driven inflammation *in vivo*, we tested this compound in a TNF-induced SIRS model.[5, 36] The compound was intragastrically administered 2 h before intravenous injection of mTNF-α. We found that compound **42** significantly protected mice from hypothermia and death at the doses of 5, 25, or 50 mg/kg (Figure 6A and B), which was much more effective than TAK-632 and its previous reported analogue compound **16** to protect mice from death and hypothermia.[36]

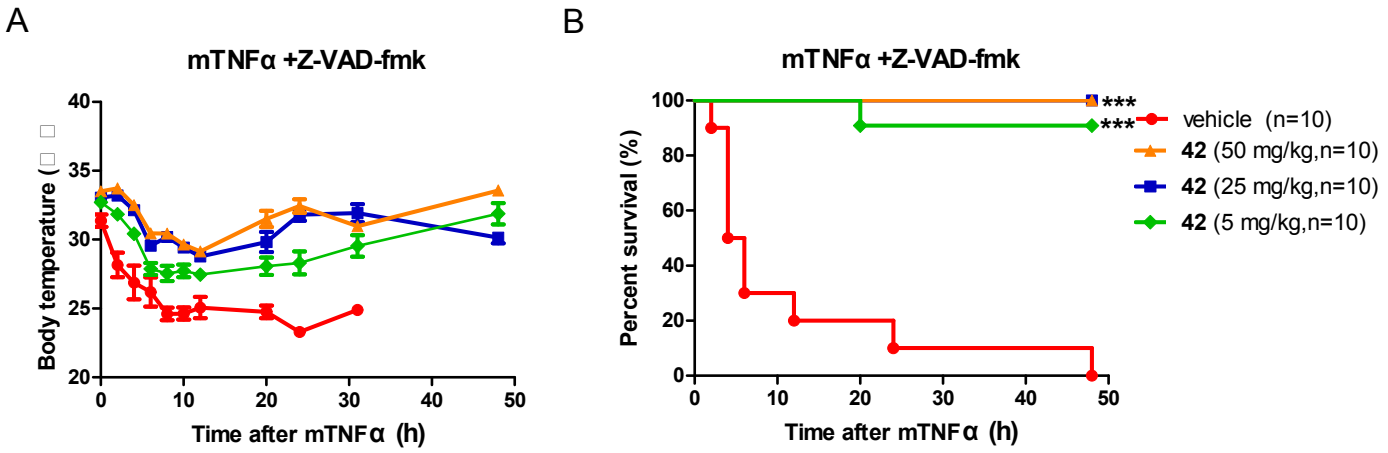

Figure 6. Compound **42** protected mice from SIRS. (A) The body temperature and (B) survival curve of C57BL/6 female mice (n=10 per group) injected with mTNF-α (400 μg/kg) after pretreatment with different doses of compound **42** (5, 25 and 50 mg/kg). ***$p < 0.0005$, treatment group versus vehicle.

Compound 42 has favorable and drug-like pharmacokinetic properties in rats.

The pharmacokinetic (PK) characteristics of compound **42** in rats was evaluated. The key p.o. and i.v. administration PK parameters are summarized in Table 5. After a single i.v. administration with 1 mg/kg compound **42**, the half time ($t_{1/2}$), the clearance rate (CL) and apparent distribution volume (V_{ss}) of **42** are 15.4 h, 2.6 mL/min/kg, and 3.49 L/kg, respectively. When **42** was administrated by oral route at 5 mg/kg, its maximum plasma concentration (C_{max}) is 345 ng/mL. Compound **42** had a favorable oral bioavailability (F) of 25.2%, suggesting a drug-like property. In addition, no apparent adverse effects were observed in rat.

Table 5. PK Profile of compound **42**[a]

Parameter	1 mg/kg (i.v.)	5 mg/kg (p.o.)
$T_{1/2}$ (h)	15.4 ± 1.0	15.2 ± 2.8
T_{max} (h)	0.083	8.67 ± 1.15
C_{max} (ng/mL)	4603 ± 554	345 ± 101
AUC_{0-t} (h*ng/mL)	5563 ± 894	7014 ± 2528
$AUC_{0-\infty}$ (h*ng/mL)	6498 ± 959	9317 ± 4081
CL (mL/min/kg)	2.6 ± 0.38	-
V_{SS} (L/kg)	3.49 ± 0.74	-
F (%)	-	25.2 ± 9.1

[a] PK parameters (mean ± SD, n = 3)

CONCLUSION

In summary, novel RIPK3-selective inhibitors were successfully identified by three rounds of structural optimization starting from TAK-632 as the lead compound. An obvious SAR was derived to guide further optimizations. Most analogues significantly suppressed necroptotic cell death in both murine and human cells with low cytotoxicity. Compounds with carbamide groups exhibited promising selectivities for RIPK3 over RIPK1 kinase. Of the prepared compounds, compound **42** showed more than 60-fold selectivity for RIPK3/1 kinase and exhibited good anti-necroptotic activity with an EC_{50} value of 0.44±0.10 μM in human HT-29 cells. Molecular docking analysis explained the target selectivity of compound **42** and provided structural basis for

further optimization. Consistent with the *in vitro* kinase assays, compound **42** showed no effect on RIPK1 phosphorylation and selectively inhibited RIPK3 and MLKL phosphorylation in cells. Remarkably, compound **42** significantly protected mice from hypothermia and death at a dose of 5 mg/kg, which was much more effective than its parent chemical TAK-632. Thus, the carbamide small molecules represent promising leads for the development of novel anti-necropototic therapeutic agents.

EXPERIMENTAL SECTION

Chemistry. All starting materials were obtained from commercial sources and were analytically pure. TAK-632 (CAS#1228591-30-7) was purchased from Targetmol with a purity of 98% (Targetmol, USA). The ^{1}H NMR and ^{13}C NMR spectra were recorded on Bruker Avance 300 and 600 spectrometers (Bruker Company, Germany) using TMS as an internal standard and $CDCl_3$ or DMSO-d_6 as solvents. Chemical shifts (δ values) and coupling constants (J values) are given in ppm and hertz (Hz), respectively. The mass spectra were recorded on an Esquire 3000 LC-MS mass spectrometer. High-resolution mass spectrometry data were acquired using a Q-TOF micro mass spectrometer. TLC analyses were carried out on silica gel plates GF254 (Qindao Haiyang Chemical, China). Column chromatography separations were carried out on silica gel 200-300 mesh. The purities of the compounds were analyzed by HPLC (Agilent 1260) using a C18 column (Elite Hypersil ODS2, 4.6*250 mm, 5 μm) with 85% methanol/15% water as the mobile phase at a flow rate of 0.6 mL/min, and all final compounds exhibited purities greater than 95%.

General procedure for the preparation of compounds 7-34.

To a solution of $NaBH_4$ (20 equiv.) in EtOH (20 mL) was added MeOH (1 mL), and the intermediate (**m11-m16**) (1 equiv.) was added to this suspension at 0 °C. The mixture was stirred at 0 °C for 1 h and then warmed to room temperature for 2 h. After the addition was completed, TLC analysis indicated the reaction was complete. The solvent was removed under reduced pressure, and the residue was re-extracted with ethyl acetate. The combined organic phase was washed with brine, dried over anhydrous Na_2SO_4, filtered and concentrated under reduced pressure to give a crude intermediate (**m17-m22**), which was used directly in the next step without purification. A solution of the corresponding intermediate (**m17-m22**) (1 equiv.), carboxylic acid

derivative (1.2 equiv.) and HATU (2 equiv.) in anhydrous pyridine was stirred at 85 °C for 8 h under a nitrogen atmosphere, at which time TLC analysis indicated the reaction was completed. The solvent was removed under reduced pressure, and the residue was extracted with ethyl acetate. The organic phase was washed with brine, dried over anhydrous Na_2SO_4, filtered, and concentrated under reduced pressure to give the crude product, which was then purified by column chromatography on silica gel (petroleum ether/ethyl acetate = 1:1). The product was recrystallized using petroleum ether/ethyl acetate to give the target compounds.

N-(7-cyano-6-(4-fluoro-3-(2-(3-(trifluoromethyl)phenyl)acetamido)phenoxy)benzo[d]thiazol-2-yl)propionamide (7). White solid (28 mg, yield: 64%). ^{1}H NMR (600 MHz, DMSO-d_6) δ 12.62 (s, 1H), 10.22 (s, 1H), 7.97 (d, 1H, J = 9.0 Hz), 7.84 (s, 1H), 7.68 (s, 1H), 7.60-7.61 (m, 2H), 7.53-7.56 (m, 1H), 7.37 (t, 1H, J = 9.6 Hz), 7.06 (d, 1H, J = 9.0 Hz), 6.96-6.97 (m, 1H), 3.88 (s, 2H), 2.54 (q, 2H, J = 7.2 Hz), 1.12 (t, 3H, J = 7.8 Hz). ^{13}C NMR (150 MHz, DMSO-d_6) δ 173.61, 169.36, 157.64, 155.65, 151.37, 150.64, 149.84, 144.63, 136.93, 135.92, 133.49, 129.27, 128.94, 127.54, 126.56, 125.87, 125.14, 123.38, 116.72, 115.19, 114.39, 113.70, 95.44, 41.98, 28.41, 8.78. HRMS (ESI, positive) m/z calcd for $C_{26}H_{18}F_4N_4O_3S$ $[M+H]^+$ 543.1109, found 543.1105. HPLC analysis: retention time = 12.2 min; peak area, >95% (210, 254 nm).

N-(7-cyano-6-(4-fluoro-3-(2-(3-(trifluoromethyl)phenyl)acetamido)phenoxy)benzo[d]thiazol-2-yl)benzamide (8). White solid (23 mg, yield: 53%). ^{1}H NMR (300 MHz, DMSO-d_6) δ 12.21 (s, 1H), 10.25 (s, 1H), 8.14 (d, 2H, J = 6.6 Hz), 8.02 (d, 1H, J = 8.7 Hz), 7.87 (s, 1H), 7.57-7.68 (m, 7H), 7.38 (t, 1H, J = 9.6 Hz), 6.99-7.11 (m, 2H), 3.89 (s, 2H). HRMS (ESI, positive) m/z calcd for $C_{30}H_{18}F_4N_4O_3S$ $[M+H]^+$ 591.1109, found 591.1116. HPLC analysis: retention time = 7.9 min; peak area, >95% (210, 254 nm).

N-(7-cyano-6-(4-fluoro-3-(2-(3-(trifluoromethyl)phenyl)acetamido)phenoxy)benzo[d]thiazol-2-yl)nonanamide (9). White solid (30 mg, yield: 71%). ^{1}H NMR (300 MHz, DMSO-d_6) δ 12.66 (s, 1H), 10.23 (s, 1H), 7.98 (d, 1H, J = 9.0 Hz), 7.82-7.85 (m, 1H), 7.68 (s, 1H), 7.52-7.62 (m, 3H), 7.38 (t, 1H, J = 9.3 Hz), 7.06 (d, 1H, J = 9.0 Hz), 6.94-7.00 (m, 1H), 3.88 (s, 2H), 2.50-2.53 (m, 2H), 1.60-1.62 (m, 2H), 1.25-1.27 (m, 10H), 0.83-0.87 (m, 3H). ^{13}C NMR (75 MHz, DMSO-d_6) δ 172.92, 169.39, 157.50, 155.72, 151.78, 144.59, 136.94, 135.91, 133.52, 129.30, 128.73, 127.55, 126.65, 125.91, 123.37, 116.80, 116.53,115.25, 114.39, 113.69, 41.98,

35.03, 31.23, 28.65, 28.52, 28.48, 24.42, 22.07, 13.95. HRMS (ESI, positive) m/z calcd for $C_{32}H_{30}F_4N_4O_3S$ $[M+H]^+$ 627.2048, found 627.2055. HPLC analysis: retention time = 16.3 min; peak area, >95% (210, 254 nm).

Benzyl(7-cyano-6-(4-fluoro-3-(2-(3-(trifluoromethyl)phenyl)acetamido)phenoxy)benzo[d]thiazol-2-yl)carbamate (10). White solid (41 mg, 19%). ^{1}H NMR (300 MHz, DMSO-d_6) δ 12.54 (s, 1H), 10.22 (s, 1H), 7.94 (d, 1H, J = 9.3 Hz), 7.83 (s, 1H), 7.57-7.68 (m, 4H), 7.37-7.46 (m, 6H), 6.95-7.07 (m, 2H), 5.30 (s, 2H), 3.88 (s, 2H). HRMS (ESI, positive) m/z calcd for $C_{31}H_{20}F_4N_4O_4S$ $[M+H]^+$ 621.1214, found 621.1219. HPLC analysis: retention time = 10.1 min; peak area, >95% (210, 254 nm).

N-(7-cyano-6-(4-fluoro-3-(2-(4-nitrophenyl)acetamido)phenoxy)benzo[d]thiazol-2-yl)cyclopropanecarboxamide (11)

White solid (39 mg, yield: 93%). ^{1}H NMR (300 MHz, DMSO-d_6) δ 12.98 (s, 1H), 10.27 (s, 1H), 8.18 (d, 2H, J = 8.1 Hz), 7.98(d, 1H, J = 9 Hz), 7.83-7.84 (m, 1H), 7.58 (d, 2H, J = 8.4 Hz), 7.37 (t, 1H, J = 9.6 Hz), 7.07 (d, 1H, J = 9.0 Hz), 6.95-6.98 (m, 1H), 3.94 (s, 2H), 1.98-2.04 (m, 1H), 0.99-1.01 (m, 4H). HRMS (ESI, positive) m/z calcd for $C_{26}H_{18}FN_5O_5S$ $[M+H]^+$ 532.1085, found 532.1095. HPLC analysis: retention time = 6.9 min; peak area, >95% (210, 254 nm).

N-(7-cyano-6-(4-fluoro-3-(2-phenylacetamido)phenoxy)benzo[d]thiazol-2-yl)cyclopropanecarboxamide (12). White solid (20 mg, yield: 53%). ^{1}H NMR (300 MHz, DMSO-d_6) δ 12.99 (s, 1H), 10.15 (s, 1H), 7.98 (d, 1H, J = 9.0 Hz), 7.84-7.87 (m, 1H), 7.30-7.39 (m, 6H), 7.06 (d, 1H, J = 9.0 Hz), 6.94-6.98 (m, 1H), 1.98-2.03 (m, 1H), 0.99-1.02 (m, 4H). HRMS (ESI, positive) m/z calcd for $C_{26}H_{19}FN_4O_3S$ $[M+H]^+$ 487.1235, found 487.1235. HPLC analysis: retention time = 7.8 min; peak area, >95% (210, 254 nm).

N-(7-cyano-6-(4-fluoro-3-(2-(3-fluorophenyl)acetamido)phenoxy)benzo[d]thiazol-2-yl)cyclopropanecarboxamide (13). White solid (22 mg, yield: 55%). ^{1}H NMR (300 MHz, DMSO-d_6) δ 12.99 (s, 1H), 10.18 (s, 1H), 7.99 (d, 1H, J = 9.0 Hz), 7.83-7.86 (m, 1H), 7.31-7.40 (m, 2H), 7.04-7.15 (m, 4H), 6.95-6.99 (m, 1H), 3.78 (s, 2H), 1.98-2.03 (m, 1H), 0.99-1.02 (m, 4H); HRMS (ESI, positive) m/z calcd for $C_{26}H_{18}F_2N_4O_3S$ $[M+H]^+$ 505.1140, found 505.1148. HPLC analysis: retention time = 7.7 min; peak area, >95% (210, 254 nm).

N-(5-((7-cyano-2-(cyclopropanecarboxamido)benzo[d]thiazol-6-yl)oxy)-2-fluorophenyl)-3-(trifluoromethyl)benzamide (14). White solid (20 mg, yield: 50%). ^{1}H NMR (300 MHz, DMSO-d_6) δ 12.99 (s, 1H), 10.50 (s, 1H), 8.23-8.28 (m, 2H), 7.97-8.06 (m, 2H), 7.78 (t, 1H, J = 7.8 Hz), 7.50-7.53 (m, 1H), 7.43 (t, 1H, J = 9.6 Hz), 7.11-7.18 (m, 2H), 1.99-2.04 (m, 1H), 0.99-1.02 (m, 4H). HRMS (ESI, positive) m/z calcd for $C_{26}H_{16}F_4N_4O_3S$ $[M+H]^+$ 541.0952, found 541.0945. HPLC analysis: retention time = 8.1 min; peak area, >95% (210, 254 nm).

N-(7-cyano-6-(4-fluoro-3-(2-(2-fluoro-3-(trifluoromethyl)phenyl)acetamido)phenoxy)benzo[d]thiazol-2-yl)cyclopropanecarboxamide (15). White solid (33 mg, yield: 55%). ^{1}H NMR (300 MHz, DMSO-d_6) δ 12.95 (s, 1H), 10.28 (s, 1H), 7.98 (d, 1H, J = 9 Hz), 7.82-7.85 (m, 1H), 7.65-7.74 (m, 2H), 7.34-7.41 (m, 2H), 7.08 (d, 1H, J = 9.0 Hz), 6.95-7.00 (m, 1H), 3.96 (s, 2H), 1.98-2.03 (m, 1H), 0.98-1.01 (m, 4H). ^{19}F NMR (282 MHz, DMSO-d_6) δ -59.91 (d, J = 12.4 Hz, CF_3), -119.86 (Ar-F), -129.81 (Ar-F). HRMS (ESI, positive) m/z calcd for $C_{27}H_{17}F_5N_4O_3S$ $[M+H]^+$ 573.1014, found 573.1024. HPLC analysis: retention time = 7.1 min; peak area, >95% (210, 254 nm).

N-(6-(4-fluoro-3-(2-(3-(trifluoromethyl)phenyl)acetamido)phenoxy)benzo[d]thiazol-2-yl)cyclopropanecarboxamide (16). White solid (100 mg, yield: 56%). ^{1}H NMR (600 MHz, DMSO-d_6) δ 12.61 (s, 1H), 10.11 (s, 1H), 7.67-7.72 (m, 3H), 7.63 (d, 1H, J = 2.4 Hz), 7.59-7.61 (m, 2H), 7.53-7.56 (m, 1H), 7.26-7.29 (m, 1H), 7.10 (dd, 1H, J_1 = 2.4 Hz, J_2 = 8.4 Hz), 6.78-6.81 (m, 1H), 3.86 (s, 2H), 1.97-2.01 (m, 1H), 0.93-0.96 (m, 4H). ^{13}C NMR (150 MHz, DMSO-d_6) δ 172.71, 169.17, 157.56, 153.07, 152.78, 149.08, 144.93, 137.00, 133.45, 132.87, 129.26, 128.94, 127.15, 125.78, 125.13, 123.33, 121.45, 118.02, 116.24, 114.34, 112.99, 111.56, 41.99, 13.75, 8.61. HRMS (ESI, positive) m/z calcd for $C_{26}H_{19}F_4N_3O_3S$ $[M+H]^+$ 530.1156, found 530.1169. HPLC analysis: retention time = 9.0 min; peak area, >95% (210, 254 nm).

N-(6-(4-fluoro-3-(2-(2-(trifluoromethyl)phenyl)acetamido)phenoxy)benzo[d]thiazol-2-yl)cyclopropanecarboxamide (17). White solid (20 mg, yield: 32%). ^{1}H NMR (600 MHz, DMSO-d_6) δ 12.60 (s, 1H), 10.10 (s, 1H), 7.70 (d, 1H, J = 8.4 Hz), 7.67-7.68 (m, 2H), 7.63 (d, 1H, J = 2.4 Hz), 7.61 (t, 1H, J = 7.8 Hz), 7.44-7.49 (m, 2H), 7.28 (t, 1H, J = 9.6 Hz), 7.10 (dd, 1H, J_1 = 2.4 Hz, J_2 = 8.4 Hz), 6.78-6.80 (m, 1H), 4.00 (s, 2H), 1.97-2.01 (m, 1H), 0.94-0.95 (m, 4H); ^{13}C NMR (150 MHz, DMSO-d_6) δ 172.71, 168.76, 157.57,

153.11, 152.77, 149.02, 144.94, 133.64, 133.39, 132.87, 132.18, 127.46, 127.28, 125.57, 125.33, 123.52, 121.44, 118.03, 116.21, 114.18, 112.89, 111.58, 13.75, 8.59. ^{19}F NMR (282 MHz, DMSO-d_6) δ -58.65 (CF_3), -131.94 (Ar-*F*). HRMS (ESI, positive) m/z calcd for $C_{26}H_{19}F_4N_3O_3S$ $[M+H]^+$ 530.1156, found 530.1173. HPLC analysis: retention time = 8.7 min; peak area, >95% (210, 254 nm).

N-(6-(4-fluoro-3-(2-(2-fluoro-3-(trifluoromethyl)phenyl)acetamido)phenoxy)benzo[d]thiazol-2-yl)cyclopropanecarboxamide (18). White solid (25 mg, yield: 38%). ^{1}H NMR (600 MHz, DMSO-d_6) δ 12.60 (s, 1H), 10.17 (s, 1H), 7.66-7.72 (m, 4H), 7.63 (d, 1H, J = 2.4 Hz), 7.36 (t, 1H, J = 7.8 Hz), 7.27-7.30 (m, 1H), 7.09 (dd, 1H, J_1 = 2.4 Hz, J_2 = 9.0 Hz), 6.79-6.82 (m, 1H), 3.93 (s, 2H), 1.97-2.01 (m, 1H), 0.93-0.96 (m, 4H). ^{13}C NMR (150 MHz, DMSO-d_6) δ 172.70, 168.64, 157.57, 153.09, 152.81, 149.16, 144.95, 138.92, 132.89, 130.35, 129.88, 127.06, 126.06, 124.26, 122.45, 121.44, 120.36, 117.97, 116.24, 114.48, 113.14, 111.51, 41.51, 13.74, 8.57. ^{19}F NMR (282 MHz, DMSO-d_6) δ -59.91 (d, J = 12.4 Hz, CF_3), -119.87 (Ar-*F*), -131.79 (Ar-*F*). HRMS (ESI, positive) m/z calcd for $C_{26}H_{18}F_5N_3O_3S$ $[M+H]^+$ 548.1056, found 548.1074. HPLC analysis: retention time = 8.8 min; peak area, >95% (210, 254 nm).

N-(6-(4-fluoro-3-(2-(4-fluoro-3-(trifluoromethyl)phenyl)acetamido)phenoxy)benzo[d]thiazol-2-yl)cyclopropanecarboxamide (19). White solid (26 mg, yield: 40%). ^{1}H NMR (600 MHz, DMSO-d_6) δ 12.60 (s, 1H), 10.09 (s, 1H), 7.64-7.72 (m, 4H), 7.62 (d, 1H, J = 2.4 Hz), 7.42-7.48 (m, 1H), 7.26-7.29 (m, 1H), 7.09 (dd, 1H, J_1 = 2.4 Hz, J_2 = 9.0 Hz), 6.78-6.81 (m, 1H), 3.84 (s, 2H), 1.98-2.00 (m, 1H), 0.94-0.95 (m, 4H). ^{13}C NMR (150 MHz, DMSO-d_6) δ 172.72, 169.13, 157.79, 157.58, 153.10, 152.79, 149.08, 144.95, 136.04, 132.88, 132.74, 127.88, 127.15, 123.56, 121.75, 121.46, 118.02, 116.96, 116.20, 114.37, 112.98, 111.56, 41.11, 13.76, 8.60. ^{19}F NMR (282 MHz, DMSO-d_6) δ -59.98 (d, J = 12.1 Hz, CF_3), -119.23 (Ar-*F*), -131.83 (Ar-*F*). HRMS (ESI, positive) m/z calcd for $C_{26}H_{18}F_5N_3O_3S$ $[M+H]^+$ 548.1062, found 548.1069. HPLC analysis: retention time = 8.9 min; peak area, >95% (210, 254 nm).

N-(6-(3-(2-(2-chloro-3-(trifluoromethyl)phenyl)acetamido)-4-fluorophenoxy)benzo[d]thiazol-2-yl)cyclopropanecarboxamide (20). White solid (21 mg, yield: 31%). ^{1}H NMR (600 MHz, DMSO-d_6) δ 12.60 (s, 1H), 10.19 (s, 1H), 7.75 (d, 1H, J = 7.8 Hz), 7.70-7.72 (m, 3H), 7.62 (d, 1H, J = 3 Hz), 7.50 (t, 1H, J = 7.8 Hz), 7.26-7.30 (m, 1H), 7.10 (dd, 1H, J_1 = 2.4 Hz, J_2 = 8.4 Hz), 6.78-6.81 (m, 1H), 4.06 (s, 2H), 1.97-2.00 (m,

1H), 0.94-0.95 (m, 4H). ^{13}C NMR (150 MHz, DMSO-d_6) δ 172.72, 168.19, 157.59, 153.14, 152.78, 149.00, 144.96, 136.73, 136.45, 132.89, 131.31, 127.26, 126.93, 126.43, 123.91, 122.10, 121.45, 118.03, 116.24, 114.23, 112.89, 111.59, 40.49, 13.76, 8.60. HRMS (ESI, positive) m/z calcd for $C_{26}H_{18}ClF_4N_3O_3S$ $[M+H]^+$ 564.0766, found 564.0767. HPLC analysis: retention time = 9.3 min; peak area, >95% (210, 254 nm).

N-(6-(3-(2-(3,5-bis(trifluoromethyl)phenyl)acetamido)-4-fluorophenoxy)benzo[d]thiazol-2-yl)cyclopropanecarboxamide (21). White solid (32 mg, yield: 46%). ^{1}H NMR (600 MHz, DMSO-d_6) δ 12.59 (s, 1H), 10.15 (s, 1H), 8.01 (s, 2H), 7.98 (s, 1H), 7.71 (d, 1H, J = 9.0 Hz), 7.65-7.67 (m, 1H), 7.62 (d, 1H, J = 2.4 Hz), 7.27-7.30 (m, 1H), 7.09 (dd, 1H, J_1 = 3.0 Hz, J_2 = 9.0 Hz), 6.79-6.82 (m, 1H), 3.31 (s, 2H), 1.97-2.00 (m, 1H), 0.93-0.96 (m, 4H). ^{13}C NMR (150 MHz, DMSO-d_6) δ 172.71, 168.12, 157.58, 157.39, 153.11, 152.79, 149.54, 144.95, 136.93, 132.89, 127.12, 125.78, 124.72, 124.55, 123.64, 121.84, 121.44, 118.01, 116.24, 114.37, 112.96, 111.56, 35.46, 13.75, 8.59. ^{19}F NMR (282 MHz, DMSO-d_6) δ -61.24 (CF_3), -131.72 (Ar-F). HRMS (ESI, positive) m/z calcd for $C_{27}H_{18}F_7N_3O_3S$ $[M+H]^+$ 598.1024, found 598.1032. HPLC analysis: retention time = 11.4 min; peak area, >95% (210, 254 nm).

N-(6-(3-(2-(3,4-dimethylphenyl)acetamido)-4-fluorophenoxy)benzo[d]thiazol-2-yl)cyclopropanecarboxamide (22).

White solid (26 mg, yield: 45%). ^{1}H NMR (300 MHz, DMSO-d_6) δ 12.63 (s, 1H), 9.96 (s, 1H), 7.70 (d, 1H, J = 8.7 Hz), 7.62 (d, 1H, J = 2.1 Hz), 7.26 (t, 1H, J = 9.6 Hz), 6.99-7.11 (m, 4H), 6.76-6.80 (m, 1H), 3.63 (s, 2H), 2.15-2.16 (m, 6H), 1.98-2.02 (m, 1H), 0.94-0.95 (m, 4H). ^{13}C NMR (75 MHz, DMSO-d_6) δ 172.75, 170.02, 157.60, 153.10, 152.82, 148.99, 144.96, 135.90, 134.28, 132.92, 132.91, 130.27, 129.36, 127.41, 126.47, 121.48, 118.06, 116.18, 114.08, 112.86, 111.59, 42.26, 19.35, 18.95, 13.80, 8.67. HRMS (ESI, positive) m/z calcd for $C_{27}H_{24}FN_3O_3S$ $[M+H]^+$ 490.1595, found 490.1597. HPLC analysis: retention time = 7.2 min; peak area, >95% (210, 254 nm).

N-(6-(4-fluoro-3-(2-(3-nitrophenyl)acetamido)phenoxy)benzo[d]thiazol-2-yl)cyclopropanecarboxamide (23). White solid (22 mg, yield: 33%). ^{1}H NMR (600 MHz, DMSO-d_6) δ 12.59 (s, 1H), 10.14 (s, 1H), 8.20 (s, 1H), 8.09-8.11 (m, 1H), 7.75 (d, 1H, J = 7.8 Hz), 7.70-7.71 (m, 2H), 7.59-7.62 (m, 2H), 7.28 (t, 1H, J = 10.2 Hz), 7.09 (dd, 1H, J_1 = 2.4 Hz, J_2 = 8.4 Hz), 6.78-6.81 (m, 1H), 3.92 (s, 2H), 1.97-2.00 (m, 1H), 0.94-0.95 (m,

4H). ^{13}C NMR (150 MHz, DMSO-d_6) δ 172.71, 168.93, 157.57, 153.11, 152.76, 149.02, 147.64, 144.94, 137.76, 136.17, 132.87, 129.65, 127.13, 123.97, 121.63, 121.45, 118.03, 116.23, 114.32, 112.88, 111.57, 41.75, 13.75, 8.60. HRMS (ESI, positive) m/z calcd for $C_{25}H_{19}FN_4O_5S$ $[M+H]^+$ 507.1127, found 507.1151. HPLC analysis: retention time = 8.2 min; peak area, >95% (210, 254 nm).

N-(6-(4-fluoro-3-(2-(m-tolyl)acetamido)phenoxy)benzo[d]thiazol-2-yl)cyclopropanecarboxamide (24). White solid (21 mg, yield: 38%). ^{1}H NMR (600 MHz, DMSO-d_6) δ 12.60 (s, 1H), 9.98 (s, 1H), 7.71 (d, 1H, J = 8.4 Hz), 7.62 (d, 1H, J = 2.4 Hz), 7.24-7.28 (m, 1H), 7.18 (t, 1H, J = 7.8 Hz), 7.08-7.11 (m, 3H), 7.02 (d, 1H, J = 7.2 Hz), 6.77-6.79 (m, 1H), 3.67 (s, 2H), 2.26 (s, 3H), 1.98-2.00 (m, 1H), 0.94-0.95 (m, 4H). ^{13}C NMR (150 MHz, DMSO-d_6) δ 172.70, 169.78, 157.56, 153.05, 152.79, 148.99, 144.92, 137.28, 135.53, 132.87, 129.75, 128.14, 127.33, 127.14, 126.17, 121.44, 118.02, 116.16, 114.16, 112.89, 111.55, 42.53, 20.92, 13.75, 8.60. HRMS (ESI, positive) m/z calcd for $C_{26}H_{22}FN_3O_3S$ $[M+H]^+$ 476.1439, found 476.1449. HPLC analysis: retention time = 9.3 min; peak area, >95% (210, 254 nm).

N-(6-(4-fluoro-3-(2-(3-methoxyphenyl)acetamido)phenoxy)benzo[d]thiazol-2-yl)cyclopropanecarboxamide (25). White solid (30 mg, yield: 52%). ^{1}H NMR (300 MHz, DMSO-d_6) δ 12.62 (s, 1H), 10.01 (s, 1H), 7.68-7.73 (m, 2H), 7.63 (d, 1H, J = 2.4 Hz), 7.18-7.30 (m, 2H), 7.10 (dd, 1H, J_1 = 2.4 Hz, J_2 = 8.7 Hz), 6.85-6.88 (m, 2H), 6.76-6.81 (m, 2H), 3.72 (s, 3H), 3.68 (s, 2H), 1.97-2.01 (m, 1H), 0.94-0.96 (m, 4H). ^{13}C NMR (75 MHz, DMSO-d_6) δ 172.75, 169.64, 159.18, 157.59, 153.07, 152.80, 149.04, 144.95, 137.12, 132.89, 129.30, 127.32, 121.49, 121.38, 118.06, 116.23, 114.90, 114.21, 112.92, 111.98, 111.60, 54.94, 42.66, 13.79, 8.66. HRMS (ESI, positive) m/z calcd for $C_{26}H_{22}FN_3O_4S$ $[M+H]^+$ 492.1388, found 492.1399. HPLC analysis: retention time = 8.4 min; peak area, >95% (210, 254 nm).

N-(6-(4-fluoro-3-(2-(3-(trifluoromethoxy)phenyl)acetamido)phenoxy)benzo[d]thiazol-2-yl)cyclopropanecarboxamide (26). White solid (32 mg, yield: 49%). ^{1}H NMR (300 MHz, DMSO-d_6) δ 12.63 (s, 1H), 10.11 (s, 1H), 7.63-7.73 (m, 3H), 7.44 (t, 1H, J = 7.8 Hz), 7.22-7.34 (m, 4H), 7.10 (d, 1H, J = 8.4 Hz), 6.78-6.81 (m, 1H), 3.80 (s, 1H), 1.99-2.01 (m, 1H), 0.93-0.95 (m, 4H). ^{13}C NMR (75 MHz, DMSO-d_6) δ 172.75, 169.16, 157.61, 153.13, 152.79, 149.09, 148.30, 144.97, 138.32, 132.91, 130.12, 128.44, 127.19, 121.66, 121.49, 119.12, 118.39, 118.07, 116.27, 114.40, 112.99, 111.62, 42.01, 13.79, 8.66. ^{19}F NMR (282

MHz, DMSO-d_6) δ -56.66 (OCF_3), -131.82 (Ar-*F*). HRMS (ESI, positive) m/z calcd for $C_{26}H_{19}F_4N_3O_4S$ $[M+H]^+$ 546.1105, found 546.1121. HPLC analysis: retention time = 9.3 min; peak area, >95% (210, 254 nm).

N-(6-(4-fluoro-3-(2-(3-hydroxyphenyl)acetamido)phenoxy)benzo[d]thiazol-2-yl)cyclopropanecarboxamide (27). White solid (26 mg, yield: 46%). ^{1}H NMR (600 MHz, DMSO-d_6) δ 12.61 (s, 1H), 9.97 (s, 1H), 9.31 (s, 1H), 7.71-7.73 (m, 2H), 7.63 (d, 1H, J = 2.4 Hz), 7.24-7.28 (m, 1H), 7.06-7.11 (m, 2H), 6.76-6.79 (m, 1H), 6.71-6.73 (m, 2H), 6.61-6.63 (m, 1H), 3.62 (s, 2H) 1.98-2.00 (m, 1H), 0.94-0.96 (m, 4H). ^{13}C NMR (150 MHz, DMSO-d_6) δ 172.73, 169.76, 157.58, 157.25, 153.07, 152.81, 148.98, 144.95, 136.91, 132.89, 129.19, 127.36, 121.47, 119.75, 118.05, 116.18, 116.00, 114.12, 113.56, 112.85, 111.58, 42.65, 13.78, 8.63. HRMS (ESI, positive) m/z calcd for $C_{25}H_{20}FN_3O_4S$ $[M+H]^+$ 478.1231, found 478.1244. HPLC analysis: retention time = 7.2 min; peak area, >95% (210, 254 nm).

N-(6-(3-(2-(3-cyanophenyl)acetamido)-4-fluorophenoxy)benzo[d]thiazol-2-yl)cyclopropanecarboxamide (28). White solid (32 mg, yield: 55%). ^{1}H NMR (300 MHz, DMSO-d_6) δ 12.62 (s, 1H), 10.12 (s, 1H), 7.70-7.74 (m, 4H), 7.62-7.64 (m, 2H), 7.51 (t, 1H, J = 7.8 Hz), 7.28 (t, 1H, J = 9.3 Hz), 7.09 (dd, 1H, J_1 = 2.4 Hz, J_2 = 8.7 Hz), 6.77-6.82 (m, 1H), 3.83 (s, 2H), 1.98-2.01 (m, 1H), 0.93-0.95 (m, 4H). ^{13}C NMR (75 MHz, DMSO-d_6) δ 172.77, 169.04, 157.61, 153.12, 152.80, 149.06, 144.97, 137.24, 134.42, 132.92, 130.48, 129.49, 127.19, 121.50, 118.78, 118.08, 116.27, 114.36, 112.96, 111.62, 111.20, 41.76, 13.81, 8.68. HRMS (ESI, positive) m/z calcd for $C_{26}H_{19}FN_4O_3S$ $[M+H]^+$ 487.1352, found 487.1244. HPLC analysis: retention time = 7.1 min; peak area, >95% (210, 254 nm).

N-(6-(4-fluoro-3-(2-(6-(trifluoromethyl)pyridin-2-yl)acetamido)phenoxy)benzo[d]thiazol-2-yl)cyclopropanecarboxamide (29). White solid (30 mg, yield: 41%). ^{1}H NMR (300 MHz, DMSO-d_6) δ 12.62 (s, 1H), 10.21 (s, 1H), 8.04 (t, 1H, J = 7.8 Hz), 7.63-7.78 (m, 5H), 7.29 (t, 1H, J = 9.6 Hz), 7.10 (dd, 1H, J_1 = 2.1 Hz, J_2 = 8.7 Hz), 6.79-6.83 (m, 1H), 4.08 (s, 2H), 1.98-2.01 (m, 1H), 0.93-0.95 (m, 4H). ^{13}C NMR (75 MHz, DMSO-d_6) δ 172.75, 168.21, 157.62, 156.77, 153.16, 152.78, 148.99, 145.86, 144.98, 138.75, 132.91, 128.05, 127.14, 121.58, 121.49, 118.90, 118.09, 116.28, 114.23, 112.84, 111.64, 44.68, 13.79, 8.66. ^{19}F NMR (282 MHz, DMSO-d_6) δ -66.37 (*C*F_3), -131.96 (Ar-*F*). HRMS (ESI, positive) m/z calcd for $C_{25}H_{18}F_4N_4O_3S$ $[M+H]^+$ 531.1109, found 531.1120. HPLC analysis: retention time = 8.5 min; peak area, >95% (210, 254 nm).

N-(6-(4-fluoro-3-(2-(pyridin-2-yl)acetamido)phenoxy)benzo[d]thiazol-2-yl)cyclopropanecarboxamide (30). White solid (23 mg, yield: 42%). ^{1}H NMR (600 MHz, DMSO-d_6) δ 12.60 (s, 1H), 10.21 (s, 1H), 8.49 (d, 1H, J = 3.6 Hz), 7.70-7.76 (m, 3H), 7.63 (d, 1H, J = 2.4 Hz), 7.36 (d, 1H, J = 7.8 Hz), 7.25-7.29 (m, 2H), 7.10 (dd, 1H, J_1 = 2.4 Hz, J_2 = 9.0 Hz), 6.77-6.80 (m, 1H), 3.93 (s, 2H), 1.97-2.01 (m, 1H), 0.94-0.95 (m, 4H). ^{13}C NMR (150 MHz, DMSO-d_6) δ 172.71, 168.67, 157.56, 155.65, 153.09, 152.79, 148.88, 148.83, 144.93, 136.66, 132.87, 127.31, 124.03, 121.93, 121.46, 118.04, 116.15, 114.06, 112.60, 111.57, 45.05, 13.75, 8.61. HRMS (ESI, positive) m/z calcd for $C_{24}H_{19}FN_4O_3S$ $[M+H]^+$ 463.1325, found 463.1248. HPLC analysis: retention time = 7.7 min; peak area, >95% (210, 254 nm).

N-(6-(3-(2-(benzo[d][1,3]dioxol-5-yl)acetamido)-4-fluorophenoxy)benzo[d]thiazol-2-yl)cyclopropanecarboxamide (31). White solid (30 mg, yield: 50%). ^{1}H NMR (300 MHz, DMSO-d_6) δ 12.62 (s, 1H), 9.96 (s, 1H), 7.70-7.73 (m, 2H), 7.62 (d, 1H, J = 2.1 Hz), 7.26 (t, 1H, J = 10.2 Hz), 7.10 (dd, 1H, J_1 = 2.4 Hz, J_2 = 8.7 Hz), 6.74-6.86 (m, 4H), 5.96 (s, 2H), 3.62 (s, 2H), 1.98-2.01 (m, 1H), 0.93-0.95 (m, 4H). ^{13}C NMR (75 MHz, DMSO-d_6) δ 172.75, 169.90, 157.59, 153.10, 152.81, 148.99, 147.12, 145.94, 144.95, 132.89, 129.26, 127.35, 122.21, 121.49, 118.07, 116.21, 114.21, 112.85, 111.61, 109.59, 108.06, 100.79, 42.18, 13.79, 8.66. HRMS (ESI, positive) m/z calcd for $C_{26}H_{20}FN_3O_5S$ $[M+H]^+$ 506.1180, found 506.1189. HPLC analysis: retention time = 8.0 min; peak area, >95% (210, 254 nm).

N-(6-(4-fluoro-3-(2-(1-methyl-1H-indol-3-yl)acetamido)phenoxy)benzo[d]thiazol-2-yl)cyclopropanecarboxamide (32). White solid (25 mg,, yield: 41%). ^{1}H NMR (600 MHz, DMSO-d_6) δ 12.59 (s, 1H), 9.90 (s, 1H), 7.69-7.72 (m, 2H), 7.62 (d, 1H, J = 2.4 Hz), 7.58 (d, 1H, J = 7.8 Hz), 7.37 (d, 1H, J = 8.4 Hz), 7.24-7.27 (m, 1H), 7.21 (s, 1H), 7.11-7.14 (m, 1H), 7.09 (dd, 1H, J_1 = 3.0 Hz, J_2 = 9.0 Hz), 6.99-7.01 (m, 1H), 6.75-6.78 (m, 1H), 3.80 (s, 2H), 3.74 (s, 3H), 1.98-2.01 (m, 1H), 0.93-0.96 (m, 4H). ^{13}C NMR (150 MHz, DMSO-d_6) δ 172.70, 170.17, 157.54, 153.04, 152.79, 148.97, 144.90, 136.47, 132.85, 128.24, 127.47, 121.44, 121.07, 118.80, 118.47, 118.01, 116.12, 114.00, 112.82, 111.53, 109.50, 107.45, 32.87, 32.22, 13.74, 8.59. HRMS (ESI, positive) m/z calcd for $C_{28}H_{23}FN_4O_3S$ $[M+H]^+$ 515.1548, found 515.1560. HPLC analysis: retention time = 7.7 min; peak area, >95% (210, 254 nm).

N-(6-(4-fluoro-3-(3-(3-(trifluoromethyl)phenyl)propanamido)phenoxy)benzo[d]thiazol-2-yl)cyclopropanecarboxamide (33). White solid (25 mg, yield: 39%). ^{1}H NMR (600 MHz, DMSO-d_6) δ 12.61 (s, 1H), 9.79 (s, 1H), 7.73 (d, 1H, J = 8.4 Hz), 7.66-7.67 (m, 1H), 7.63 (d, 1H, J = 2.4 Hz), 7.59 (s, 1H), 7.48-7.54 (m, 3H), 7.23-7.26 (m, 1H), 7.10 (dd, 1H, J_1 = 2.4 Hz, J_2 = 8.4 Hz), 6.76-6.79 (m, 1H), 2.96 (t, 2H, J = 7.8 Hz), 2.74 (t, 2H, J = 7.8 Hz), 1.98-2.01 (m, 1H), 0.94-0.96 (m, 4H). ^{13}C NMR (150 MHz, DMSO-d_6) δ 172.73, 170.76, 157.59, 153.09, 152.76, 149.00, 144.97, 142.46, 132.89, 132.51, 129.22, 128.93, 127.22, 124.77, 124.28, 122.71, 121.46, 118.09, 116.15, 114.04, 112.97, 111.62, 36.99, 30.32, 13.76, 8.60. HRMS (ESI, positive) m/z calcd for $C_{27}H_{21}F_4N_3O_3S$ $[M+H]^+$ 544.1313, found 544.1324. HPLC analysis: retention time = 9.5 min; peak area, >95% (210, 254 nm).

N-(5-((2-(cyclopropanecarboxamido)benzo[d]thiazol-6-yl)oxy)-2-fluorophenyl)-1-(3-(trifluoromethyl)phenyl)cyclopropanecarboxamide (34). White solid (18 mg, yield: 27%). ^{1}H NMR (300 MHz, DMSO-d_6) δ 12.64 (s, 1H), 8.62 (s, 1H), 7.58-7.75 (m, 6H), 7.28-7.31 (m, 1H), 7.22 (t, 1H, J = 9.9 Hz), 7.10 (dd, 1H, J_1 = 2.7 Hz, J_2 =9.0 Hz), 6.81-6.87 (m, 1H), 1.97-2.01 (m, 1H), 1.48-1.51 (m, 2H), 1.18-1.22 (m, 2H), 0.94-0.97 (m, 4H). ^{13}C NMR (75 MHz, DMSO-d_6) δ 172.76, 170.78, 157.64, 153.06, 152.69, 150.36, 145.03, 140.76, 134.13, 132.90, 129.77, 129.38, 126.81, 126.38, 124.27, 124.13, 121.52, 118.16, 116.28, 115.45, 114.53, 111.76, 30.85, 15.48, 13.78, 8.67. HRMS (ESI, positive) m/z calcd for $C_{28}H_{21}F_4N_3O_3S$ $[M+H]^+$ 556.1313, found 556.1316. HPLC analysis: retention time = 9.3 min; peak area, >95% (210, 254 nm).

Procedure for the preparation of N-(6-(4-fluoro-3-(3-(trifluoromethyl)phenylsulfonamido)phenoxy)benzo[d]thiazol-2-yl)cyclopropanecarboxamide (35).

A solution of intermediate **m21** (1 equiv.) in anhydrous pyridine was cooled to 0 °C under a nitrogen atmosphere. The 3-(trifluoromethyl)benzene-1-sulfonyl chloride (2 equiv.) was added, and then the mixture was stirred at 0 °C overnight. After the addition was completed, TLC analysis indicated the reaction was complete. The solvent was removed under reduced pressure, and the residue was extracted with ethyl acetate. The organic layer was washed with brine, dried over anhydrous Na_2SO_4, filtered and concentrated under reduced pressure. The crude product was purified by column chromatography on silica gel (petroleum ether/ethyl acetate = 1:1) to provide target compound **35**. White solid (30 mg, yield: 45%). ^{1}H NMR (600 MHz, DMSO-d_6) δ 12.64 (s, 1H),

10.48 (s, 1H), 8.01 (d, 1H, J = 7.8 Hz), 7.94-7.98 (m, 2H), 7.79 (t, 1H, J = 7.8 Hz), 7.71 (d, 1H, J = 8.4 Hz), 7.60 (d, 1H, J = 2.4 Hz), 7.20 (t, 1H, J = 9.6 Hz), 7.01 (dd, 1H, J_1 = 2.4 Hz, J_2 = 8.4 Hz), 6.88-6.91 (m, 1H), 6.74-6.75 (m, 1H), 1.98-2.02 (m, 1H), 0.95-0.96 (m, 4H). ^{13}C NMR (150 MHz, DMSO-d_6) δ 172.78, 157.77, 153.50, 152.08, 151.55, 145.24, 140.74, 132.92, 130.84, 130.56, 129.94, 129.72, 124.66, 123.24, 123.10, 121.50, 118.15, 117.17, 168.98, 115.54, 111.98, 13.77, 8.63. HRMS (ESI, positive) m/z calcd for $C_{24}H_{17}F_4N_3O_4S_2$ $[M+H]^+$ 552.0669, found 552.0669. HPLC analysis: retention time = 7.2 min; peak area, >95% (210, 254 nm).

General procedure for the preparation of compounds 36-37.

To a solution of intermediate **m21** and the appropriate benzaldehyde derivative (1 equiv.) in MeOH was added a catalytic amount of acetic acid. The solution was stirred at room temperature for 12 h. Then, $NaBH_3CN$ (2 equiv.) was added, and the mixture was stirred at room temperature for another 12 h, after which TLC analysis indicated the reaction was completed. The solvent was removed under reduced pressure, and the residue was re-extracted with ethyl acetate. The combined organic phase was washed with brine and dried over anhydrous Na_2SO_4. The crude product was purified by column chromatography on silica gel (DCM/MeOH = 100:1) to provide target compounds **36-37**.

N-(6-(3-((benzo[d][1,3]dioxol-5-ylmethyl)amino)-4-fluorophenoxy)benzo[d]thiazol-2-yl)cyclopropanecarboxamide (36). White solid (15 mg, yield: 26%). ^{1}H NMR (300 MHz, DMSO-d_6) δ 12.59 (s, 1H), 7.64 (d, 1H, J = 8.7 Hz), 7.47 (d, 1H, J = 2.4 Hz), 6.95-7.01 (m, 2H), 6.84-6.85 (m, 1H), 6.69-6.78 (m, 2H), 6.30-6.41 (m, 1H), 6.23 (dd, 1H, J_1 = 2.7 Hz, J_2 =7.5 Hz), 6.05-6.10 (m, 1H), 5.95 (s, 2H), 4.17 (d, 2H, J = 5.4 Hz), 1.97-2.01 (m, 1H), 0.94-0.96 (m, 4H). ^{13}C NMR (75 MHz, DMSO-d_6) δ 172.70, 157.31, 153.77, 153.08, 147.31, 147.08, 145.94, 144.56, 137.52, 133.38, 132.72, 121.21, 119.99, 117.75, 114.77, 111.00, 107.86, 107.36, 104.20, 103.08, 100.75, 45.54, 13.75, 8.63. HRMS (ESI, positive) m/z calcd for $C_{25}H_{20}FN_3O_4S$ $[M+H]^+$ 478.1231, found 478.1240. HPLC analysis: retention time = 11.0 min; peak area, >95% (210, 254 nm).

N-(6-(4-fluoro-3-((3-(trifluoromethyl)benzyl)amino)phenoxy)benzo[d]thiazol-2-yl)cyclopropanecarboxamide (37). White solid (19 mg, yield: 32%). ^{1}H NMR (300 MHz, DMSO-d_6) δ 12.59 (s, 1H), 7.44-7.65 (m, 6H), 6.91-7.05 (m, 2H), 6.55 (t, 1H, J = 4.5 Hz), 6.25 (dd, 1H, J_1 = 2.4 Hz, J_2 =7.2 Hz), 6.08-6.10 (m, 1H), 4.38 (d, 2H, J = 6.0 Hz), 1.97-2.01 (m, 1H), 0.93-0.95 (m, 4H). ^{13}C NMR (75 MHz, DMSO-

d_6) δ 172.69, 157.27, 153.73, 153.14, 147,14, 144.53, 141.26, 137.36, 132.72, 131.06, 129.25, 127.45, 123.46, 122.47, 121.18, 117.52, 115.01, 110.84, 104.67, 103.10, 45.21, 13.71, 8.62. HRMS (ESI, positive) m/z calcd for $C_{25}H_{19}F_4N_3O_2S$ $[M-H]^-$ 500.1061, found 500.1046. HPLC analysis: retention time = 7.1 min; peak area, >95% (210, 254 nm).

General procedure for preparing compounds 38-42.

A solution of intermediate **m21** (1 equiv.) and the appropriate phenyl isocyanate derivative (1.5 equiv.) in DMF, MeCN or DMSO was stirred at room temperature for 24 h. After this time, TLC analysis indicated the reaction was completed. The mixture was poured into water and extracted with ethyl acetate. The organic layer was washed with brine and dried over anhydrous Na_2SO_4. The solvent was removed under reduced pressure, and the crude product was purified by column chromatography on silica gel (DCM/MeOH = 100:2) to provide target compounds **38-42**.

N-(6-(4-fluoro-3-(3-(3-methoxyphenyl)ureido)phenoxy)benzo[d]thiazol-2-yl)cyclopropanecarboxamide (38). Light-yellow solid (32 mg, yield: 54%). ^{1}H NMR (600 MHz, DMSO-d_6) δ 12.61 (s, 1H), 9.11 (s, 1H), 8.65 (d, 1H, J = 2.4 Hz), 7.93 (dd, 1H, J_1 = 3.0 Hz, J_2 = 6.6 Hz), 7.73 (d, 1H, J = 8.4 Hz), 7.66 (d, 1H, J = 2.4 Hz), 7.24-7.27 (m, 1H), 7.17 (t, 1H, J = 7.8 Hz), 7.11 (dd, 1H, J_1 = 3.0, J_2 = 9.0 Hz), 7.10 (t, 1H, J = 2.4 Hz), 6.89-6.90 (m, 1H), 6.63-6.66 (m, 1H), 6.55 (dd, 1H, J_1 = 2.4 Hz, J_2 = 8.4 Hz), 3.71 (s, 3H), 1.98-2.00 (m, 1H), 0.94-0.96 (m, 4H). ^{13}C NMR (150 MHz, DMSO-d_6) δ 172.69, 159.69, 157.47, 153.17, 153.10, 151.88, 147.78, 144.79, 140.33, 132.86, 129.62, 128.69, 121.43, 117.84, 115.64, 111.60, 111.25, 110.47, 110.19, 107.64, 103.91, 54.92, 13.74, 8.59. HRMS (ESI, positive) m/z calcd for $C_{25}H_{21}FN_4O_4S$ $[M+H]^+$ 493.1340, found 493.1350. HPLC analysis: retention time = 9.2 min; peak area, >95% (210, 254 nm).

N-(6-(4-fluoro-3-(3-(m-tolyl)ureido)phenoxy)benzo[d]thiazol-2-yl)cyclopropanecarboxamide (39). Light-yellow solid (32 mg, yield: 56%). ^{1}H NMR (600 MHz, DMSO-d_6) δ 12.62 (s, 1H), 9.03 (s, 1H), 8.66 (s, 1H), 7.95-7.96 (m, 1H), 7.72 (d, 1H, J = 8.4 Hz), 7.64 (s, 1H), 7.11-7.25 (m, 5H), 6.78 (d, 1H, J = 7.2 Hz), 6.63-6.64 (m, 1H), 2.25 (s, 3H), 1.98-2.01 (m, 1H), 0.94-0.95 (m, 4H). ^{13}C NMR (150 MHz, DMSO-d_6) δ 172.71, 157.51, 153.26, 153.12, 151.95, 147.74, 144.82, 139.08, 138.07, 132.90, 128.87, 128.67, 122.94, 121.44, 118.67, 117.89,

115.56, 115.36, 111.47, 111.30, 110.04, 21.14, 13.78, 8.61. HRMS (ESI, positive) m/z calcd for $C_{25}H_{21}FN_4O_3S$ $[M+H]^+$ 477.1386, found 477.1400. HPLC analysis: retention time = 10.2 min; peak area, >95% (210, 254 nm).

Ethyl3-(3-(5-((2-(cyclopropanecarboxamido)benzo[d]thiazol-6-yl)oxy)-2-fluorophenyl)ureido)benzoate (40). White solid (35 mg, yield: 55%). ^{1}H NMR (600 MHz, DMSO-d_6) δ 12.62 (s, 1H), 9.34 (s, 1H), 8.66 (s, 1H), 8.07 (t, 1H, J = 2.1 Hz), 7.91 (dd, 1H, J_1 = 3.0 Hz, J_2 = 7.2 Hz), 7.73 (d, 1H, J = 9 Hz), 7.65 (d, 1H, J = 2.4 Hz), 7.56-7.61 (m, 2H), 7.41 (t, 1H, J = 7.8 Hz), 7.24-7.28 (m, 1H), 7.13 (dd, 1H, J_1 = 3.0 Hz, J_2 = 9.0 Hz), 6.65-6.68 (m, 1H), 4.29 (q, 2H, J = 7.2 Hz), 1.97-2.01 (m, 1H), 1.30 (t, 3H, J = 7.2 Hz), 0.94-0.96 (m, 4H). ^{13}C NMR (150 MHz, DMSO-d_6) δ 172.70, 165.55, 157.51, 153.31, 152.98, 151.92, 147.83, 144.86, 139.54, 132.87, 130.51, 129.27, 128.49, 122.80, 122.57, 121.45, 118.41, 117.97, 115.70, 111.74, 111.43, 110.16, 60.73, 14.10, 13.75, 8.60. HRMS (ESI, positive) m/z calcd for $C_{27}H_{23}FN_4O_5S$ $[M+H]^+$ 535.1446, found 535.1459. HPLC analysis: retention time = 10.5 min; peak area, >95% (210, 254 nm).

N-(6-(3-(3-acetylphenyl)ureido)-4-fluorophenoxy)benzo[d]thiazol-2-yl)cyclopropanecarboxamide (41). White solid (30 mg, yield: 50%). ^{1}H NMR (600 MHz, DMSO-d_6) δ 12.61 (s, 1H), 9.32 (s, 1H), 8.69 (s, 1H), 7.98 (t, 1H, J = 1.8 Hz), 7.92 (dd, 1H, J_1 = 3.0 Hz, J_2 = 6.6 Hz), 7.73 (d, 1H, J = 9.0 Hz), 7.58-7.65 (m, 3H), 7.42 (t, 1H, J = 7.8 Hz), 7.25-7.28 (m, 1H), 7.12 (dd, 1H, J_1 =2.4 Hz, J_2 = 9.0 Hz), 6.65-6.67 (m, 1H), 2.54 (s, 1H), 1.97-2.01 (m, 1H), 0.94-0.96 (m, 4H). ^{13}C NMR (150 MHz, DMSO-d_6) δ 197.62, 172.70, 157.50, 153.26, 153.05, 151.99, 148.36, 144.83, 139.55, 137.45, 132.88, 129.26, 128.53, 122.71, 122.26, 121.45, 117.92, 117.24, 115.70, 111.78, 111.35, 110.27, 26.71, 13.75, 8.60. HRMS (ESI, positive) m/z calcd for $C_{26}H_{21}FN_4O_4S$ $[M+H]^+$ 505.1340, found 505.1351. HPLC analysis: retention time = 7.7 min; peak area, >95% (210, 254 nm).

N-(6-(3-(3-(3-bromophenyl)ureido)-4-fluorophenoxy)benzo[d]thiazol-2-yl)cyclopropanecarboxamide (42). White solid (35 mg, yield: 54%). ^{1}H NMR (600 MHz, DMSO-d_6) δ 12.61 (s, 1H), 9.27 (s, 1H), 8.71 (s, 1H), 7.89-7.91 (m, 1H), 7.79 (t, 1H, J = 1.2 Hz), 7.73 (d, 1H, J = 9.0 Hz), 7.63 (d, 1H, J = 2.4 Hz), 7.21-7.27 (m, 3H), 7.12-7.16 (m, 2H), 6.65-6.68 (m, 1H), 1.97-2.00 (m, 1H), 0.94-0.95 (m, 4H). ^{13}C NMR (150 MHz, DMSO-d_6) δ 172.71, 157.51, 153.26, 153.04, 151.83, 147.88, 144.84, 140.80, 132.88, 130.77, 128.41, 124.76, 121.75, 121.45, 120.35, 117.91, 117.02, 115.72, 111.89, 111.35, 110.31, 13.76, 8.76. HRMS (ESI, positive) m/z calcd for

$C_{24}H_{18}BrFN_4O_3S$ $[M+H]^+$ 541.0340, found 541.0346. HPLC analysis: retention time = 11.6 min; peak area, >95% (210, 254 nm).

Biology.

Reagents and antibodies. Recombinant mouse/human TNF-α and z-VAD-fmk were purchased from R&D System (Minneapolis, MN, USA). Protease inhibitor cocktail was purchased from Sigma-Aldrich (St. Louis, MO, USA). Smac mimetic (SM-164) was a gift from Dr. Zheng-gang Liu (NCI, NIH). The antibodies were obtained from commercial sources: anti-RIPK1 (610458) from BD Biosciences; anti-human phospho-RIPK1 (65746) from Cell Signaling Technology; anti-human-RIPK3 (ab56164), anti-human phospho-RIPK3 (ab209384), anti-human MLKL (ab184718), anti-human phospho-MLKL (ab187091) from Abcam; and anti-actin (A3853) from Sigma.

Cell culture. HT-29 and L929 cells were cultured in DMEM. All media were supplemented with 10% FBS (*v/v*), 2 mM L-glutamine and 100 U/mL penicillin/streptomycin. Cells were grown at 37 °C in a humidified atmosphere with 5% CO_2, and for all experiments, cells were harvested from exponentially growing cultures.

Necroptosis induction and cell viability assays. Necroptosis was induced by pretreatment with z-VAD-fmk (20 μM) and Smac mimetic (10 nM) for 30 min followed by treatment with TNF-α (20 ng/mL) for the indicated time periods. Apoptosis was induced by treatment with TNF-α (20 ng/mL) and Smac mimetic (10 nM) for the indicated time periods. After the cells were exposed to one of the above combinations, they were incubated with the test compounds at the indicated concentrations for 12 h. The cell viability was then examined using the CellTiter-Glo Luminescent Cell Viability Assay kit (Promega). The luminescence was recorded with a BioTek 312e microplate reader (BioTek Instruments, Winooski, VT).

Immunoblotting and immunoprecipitation. Cells were collected and lysed in M2 buffer (20 mM Tris, pH 7, 0.5% NP40, 250 mM NaCl, 3 mM EDTA, 3 mM EGTA, 2 mM DTT, 0.5 mM PMSF, 20 mM glycerol phosphate, 1 mM sodium vanadate, and 1 μg/mL leupeptin). Cell lysates were separated by SDS-PAGE and analyzed by immunoblotting. The dilution ratio of the antibodies used for western blotting was 1:1000. The proteins were visualized by enhanced chemiluminescence according to the manufacturer's instructions

(Amersham). For immunoprecipitation analysis, the cells were washed three times with ice-cold PBS solution and lysed in M2 buffer. The samples were precipitated with the indicated antibodies (1 μg) and protein A/G-agarose beads (Santa Cruze) by incubating at 4 °C overnight. The beads were washed four times with 1 mL of M2 buffer, the bound proteins were removed by boiling in SDS buffer, and the samples were resolved in 4%-20% SDS-polyacrylamide gels by western blotting analysis.

Kinase assays. The inhibitory effects of the test compounds on kinases were detected by a KINOMEscan™ assay. Briefly, kinase-tagged T7 phage strain lysates were tagged with DNA for qPCR detection. Binding reactions were conducted by combining the kinases, liganded affinity beads, and test compounds in 1× binding buffer (20% SeaBlock, 0.17 × PBS, 0.05% Tween 20, and 6 mM DTT). The compounds were used in the form of 10 mM solutions in 100% DMSO. Equilibrium dissociation constants (K_d values) were determined using a 10-point 3-fold compound dilution series with three DMSO control points. All reactions were performed in polypropylene 384-well plates. The assay plates were incubated at room temperature with shaking for 1 h, and the affinity beads were washed with wash buffer (1× PBS with 0.05% Tween 20). The beads were then resuspended in elution buffer (1× PBS, 0.05% Tween 20, and 0.5 μM nonbiotinylated affinity ligand) and incubated at room temperature with shaking for 30 min. The kinase concentrations in the eluates were measured by qPCR. The assays are similar for other kinases. The test compound was prepared as 40× stocks in 100% DMSO and directly diluted into the assays with the final concentration of 1000 nM.

Molecular modelling study. All the modeling studies were carried out using the Schrodinger Maestro 11.4. The PDB entry 6HHO was chosen for the RIPK1 docking study.[43] The murine RIPK3 (PDB entry: 4M69) was selected as the template to build the three-dimensional structure of human RIPK3.[42] The PDB entry 4KSP was chosen for the B-raf docking study.[37] Schrodinger Prime was used to perform the homology modeling and refinement with the default parameters. The amino-acid residues were numbered according the sequence NP_006862.[44] The protein preparation was followed our previous standard protocol.[45, 46] The Glide docking was used to dock compound into RIPK1 (docking pocket: GSK547 binding pocket), RIPK3 (docking pocket: ANP binding pocket) or B-raf (docking pocket: TAK-632 binding pocket) at the extra precision (XP). Molecular docking result is generated using PyMol (http://pymol.sourceforge.net/).

Animal experiments. All animal experiments were performed in accordance with the National Institutes of Health guidelines and approved by the Animal Care and Use Committee of the Second Military Medical University. For TNF-induced SIRS, female C57BL/6 J mice (6–8 weeks old) were purchased from Shanghai SLAC Laboratory Animal Co. (Shanghai, China) and raised in a pathogen-free environment (23 ± 2 °C and 55% ± 5% humidity). The test compounds were suspended in pH 8.0 distilled water containing 0.5% carboxymethyl cellulose sodium. Overnight-fasted mice were given the test compound (5, 25, and 50 mg/kg) by oral gavage 2 h before mTNF-α injection. z-VAD-fmk (180 μg) was intraperitoneally injected, and after 15 min, mTNF-α diluted in 272 μL of endotoxin-free PBS was intravenously injected (400 μg/kg). Then, 1 h after mTNF-α treatment, another dose of z-VAD-fmk (70 μg) was intraperitoneally injected. The body temperatures od the mice were monitored with an electric thermometer at different time points.

PK study. Male Sprague−Dawley rats (n = 3, 180-230 g, Shanghai Caerulum Pharma Discovery Co., Ltd) were used in the PK studies of compound **42**. The compound was dissolved and vortexed in 5% DMSO, 10% Tween 80, and 75% physiological saline for a concentration of 0.2 mg/mL and 1 mg/mL. The rats were housed in a room with controlled temperature and humidity and allowed free access to food and water. The male Sprague-Dawley rats were split into intravenous injection group (**42**, 1 mg/kg) and intragastric administration group (**42**, 5 mg/kg) before starting treatment. At different time points, the blood samples were collected and centrifuged at 4 °C to obtain plasma, which was stored at −80 °C until analysis by LC/MS/MS. PK parameters were determined from individual animal data using noncompartmental analysis in winNonlin 6.3.

Statistical analysis. The one-way analysis of variance was used to compare differences among groups represented by the mean values ± SD. A log-rank (Mantel-Cox) test was performed for survival curve analysis. $P < 0.05$ was considered statistically significant.

ASSOCIATED CONTENT

Supporting Information.

The Supporting Information is available free of charge on the ACS Publications website at DOI: ###. Synthetic protocols, detailed experimental procedures, ^{1}H and ^{13}C NMR spectra, HRMS spectra, and HPLC chromatograms showing the purity of the target compounds (DOCX); SMILES molecular formula strings (CSV).

AUTHOR INFORMATION

Corresponding Authors

* zclnathan@163.com (C. Zhuang); drcaizhenyu@126.com (Z. Cai); zhangwnk@hotmail.com (W. Zhang).

Author Contributions

†H.Z., L.X., and X.Q. contributed equally to this work.

Notes

The authors declare that they have no competing interests.

ACKNOWLEDGMENT

This work was funded by grants from the National Natural Science Foundation of China (81872791 to C.Z. and 81773075 to Z.C.); the Young Elite Scientists Sponsorship Program by the China Association for Science and Technology (2017QNRC061 to C.Z.); China's 1000 Young Talents Program (Z.C.); the Shanghai Municipal Commission of Health and Family Planning (2017YQ052 to C.Z.); the Key Research and Development Program of Ningxia (2018BFH02001 to W. Z. and 2018BFH02001-01, 2019BFG02017 to C.Z.); the Shanghai International Cooperation and Exchange Project (No.18410720600 to Z.C.); and the Shanghai ‘‘ChenGuang’’ Project (16CG42 to C.Z.).

ABBREVIATIONS

DMF, N,N-dimethylformamide; HATU, 2-(7-azabenzotriazol-1-yl)-N,N,N',N'-tetramethyluronium hexafluorophosphate; HPLC, high-performance liquid chromatography; IFN, interferon; MLKL, mixed lineage kinase domain-like protein; PK, pharmacokinetic; RIPK1, receptor-interacting protein kinase 1; RIPK3, receptor-interacting protein kinase 3; SAR, structure-activity relationship; SIRS, systemic inflammatory response syndrome; TC, TNF-α and cycloheximide; TCZ, TNF-α, cycloheximide and z-VAD-fmk; TFAA, trifluoroacetic anhydride; TLC, thin-layer chromatography; TLR3/4, Toll-like receptors 3/4; TNFR1, TNF receptor 1; FAS, CD95; TNFα, tumor necrosis factor; TS, TNF-α and Smac mimetic; TSZ, TNF-α, Smac mimetic and z-VAD-FMK.

REFERENCES

1. Jaattela, M.; Tschopp, J. Caspase-independent cell death in T lymphocytes. *Nat. Immunol.* **2003,** 4, 416-423.

2. Pasparakis, M.; Vandenabeele, P. Necroptosis and its role in inflammation. *Nature* **2015,** 517, 311-320.

3. Linkermann, A.; Brasen, J. H.; De Zen, F.; Weinlich, R.; Schwendener, R. A.; Green, D. R.; Kunzendorf, U.; Krautwald, S. Dichotomy between RIP1- and RIP3-mediated necroptosis in tumor necrosis factor-alpha-induced shock. *Mol. Med.* **2012,** 18, 577-586.

4. Linkermann, A.; Brasen, J. H.; Himmerkus, N.; Liu, S.; Huber, T. B.; Kunzendorf, U.; Krautwald, S. Rip1 (receptor-interacting protein kinase 1) mediates necroptosis and contributes to renal ischemia/reperfusion injury. *Kidney Int.* **2012,** 81, 751-761.

5. Duprez, L.; Takahashi, N.; Van Hauwermeiren, F.; Vandendriessche, B.; Goossens, V.; Vanden Berghe, T.; Declercq, W.; Libert, C.; Cauwels, A.; Vandenabeele, P. RIP kinase-dependent necrosis drives lethal systemic inflammatory response syndrome. *Immunity* **2011,** 35, 908-918.

6. Degterev, A.; Huang, Z.; Boyce, M.; Li, Y.; Jagtap, P.; Mizushima, N.; Cuny, G. D.; Mitchison, T. J.; Moskowitz, M. A.; Yuan, J. Chemical inhibitor of nonapoptotic cell death with therapeutic potential for ischemic brain injury. *Nat. Chem. Biol.* **2005,** 1, 112-119.

7. Lin, J.; Li, H.; Yang, M.; Ren, J.; Huang, Z.; Han, F.; Huang, J.; Ma, J.; Zhang, D.; Zhang, Z.; Wu, J.; Huang, D.; Qiao, M.; Jin, G.; Wu, Q.; Huang, Y.; Du, J.; Han, J. A role of RIP3-mediated macrophage necrosis in atherosclerosis development. *Cell Rep.* **2013,** 3, 200-210.

8. Silke, J.; Rickard, J. A.; Gerlic, M. The diverse role of RIP kinases in necroptosis and inflammation. *Nat. Immunol.* **2015,** 16, 689-697.

9. Yuan, J.; Amin, P.; Ofengeim, D. Necroptosis and RIPK1-mediated neuroinflammation in CNS diseases. *Nat. Rev. Neurosci.* **2019,** 20, 19-33.

10. Grootjans, S.; Vanden Berghe, T.; Vandenabeele, P. Initiation and execution mechanisms of necroptosis: an overview. *Cell Death Differ.* **2017,** 24, 1184-1195.

11. He, S.; Wang, L.; Miao, L.; Wang, T.; Du, F.; Zhao, L.; Wang, X. Receptor interacting protein kinase-3 determines cellular necrotic response to TNF-alpha. *Cell* **2009,** 137, 1100-1111.

12. Cho, Y. S.; Challa, S.; Moquin, D.; Genga, R.; Ray, T. D.; Guildford, M.; Chan, F. K. Phosphorylation-driven assembly of the RIP1-RIP3 complex regulates programmed necrosis and virus-induced inflammation. *Cell* **2009,** 137, 1112-1123.

13. Sun, L.; Wang, H.; Wang, Z.; He, S.; Chen, S.; Liao, D.; Wang, L.; Yan, J.; Liu, W.; Lei, X.; Wang, X. Mixed lineage kinase domain-like protein mediates necrosis signaling downstream of RIP3 kinase. *Cell* **2012,** 148, 213-227.

14. Zhao, J.; Jitkaew, S.; Cai, Z.; Choksi, S.; Li, Q.; Luo, J.; Liu, Z. G. Mixed lineage kinase domain-like is a key receptor interacting protein 3 downstream component of TNF-induced necrosis. *Proc. Natl. Acad. Sci. U S A* **2012,** 109, 5322-5327.

15. Cai, Z.; Jitkaew, S.; Zhao, J.; Chiang, H. C.; Choksi, S.; Liu, J.; Ward, Y.; Wu, L. G.; Liu, Z. G. Plasma membrane translocation of trimerized MLKL protein is required for TNF-induced necroptosis. *Nat. Cell Biol.* **2014,** 16, 55-65.

16. Chen, X.; Li, W.; Ren, J.; Huang, D.; He, W. T.; Song, Y.; Yang, C.; Li, W.; Zheng, X.; Chen, P.; Han, J. Translocation of mixed lineage kinase domain-like protein to plasma membrane leads to necrotic cell death. *Cell Res.* **2014,** 24, 105-121.

17. Dondelinger, Y.; Declercq, W.; Montessuit, S.; Roelandt, R.; Goncalves, A.; Bruggeman, I.; Hulpiau, P.; Weber, K.; Sehon, C. A.; Marquis, R. W.; Bertin, J.; Gough, P. J.; Savvides, S.; Martinou, J. C.; Bertrand, M. J.; Vandenabeele, P. MLKL compromises plasma membrane integrity by binding to phosphatidylinositol phosphates. *Cell Rep.* **2014,** 7, 971-981.

18. Wang, H.; Sun, L.; Su, L.; Rizo, J.; Liu, L.; Wang, L. F.; Wang, F. S.; Wang, X. Mixed lineage kinase domain-like protein MLKL causes necrotic membrane disruption upon phosphorylation by RIP3. *Mol. Cell* **2014,** 54, 133-146.

19. Wallach, D.; Kang, T. B.; Dillon, C. P.; Green, D. R. Programmed necrosis in inflammation: Toward identification of the effector molecules. *Science* **2016,** 352, aaf2154.

20. Teng, X.; Degterev, A.; Jagtap, P.; Xing, X.; Choi, S.; Denu, R.; Yuan, J.; Cuny, G. D. Structure-activity relationship study of novel necroptosis inhibitors. *Bioorg. Med. Chem. Lett.* **2005,** 15, 5039-5044.

21. Degterev, A.; Hitomi, J.; Germscheid, M.; Ch'en, I. L.; Korkina, O.; Teng, X.; Abbott, D.; Cuny, G. D.; Yuan, C.; Wagner, G.; Hedrick, S. M.; Gerber, S. A.; Lugovskoy, A.; Yuan, J. Identification of RIP1 kinase as a specific cellular target of necrostatins. *Nat. Chem. Biol.* **2008,** 4, 313-321.

22. Takahashi, N.; Duprez, L.; Grootjans, S.; Cauwels, A.; Nerinckx, W.; DuHadaway, J. B.; Goossens, V.; Roelandt, R.; Van Hauwermeiren, F.; Libert, C.; Declercq, W.; Callewaert, N.; Prendergast, G. C.; Degterev, A.; Yuan, J.; Vandenabeele, P. Necrostatin-1 analogues: critical issues on the specificity, activity and in vivo use in experimental disease models. *Cell Death Dis.* **2012,** 3, e437.

23. Yoshikawa, M.; Saitoh, M.; Katoh, T.; Seki, T.; Bigi, S. V.; Shimizu, Y.; Ishii, T.; Okai, T.; Kuno, M.; Hattori, H.; Watanabe, E.; Saikatendu, K. S.; Zou, H.; Nakakariya, M.; Tatamiya, T.; Nakada, Y.; Yogo, T. Discovery of 7-Oxo-2,4,5,7-tetrahydro-6 H-pyrazolo[3,4- c]pyridine derivatives as potent, orally available, and brain-penetrating receptor interacting protein 1 (RIP1) kinase inhibitors: analysis of structure-kinetic relationships. *J. Med. Chem.* **2018,** 61, 2384-2409.

24. Harris, P. A.; King, B. W.; Bandyopadhyay, D.; Berger, S. B.; Campobasso, N.; Capriotti, C. A.; Cox, J. A.; Dare, L.; Dong, X.; Finger, J. N.; Grady, L. C.; Hoffman, S. J.; Jeong, J. U.; Kang, J.; Kasparcova, V.; Lakdawala, A. S.; Lehr, R.; McNulty, D. E.; Nagilla, R.; Ouellette, M. T.; Pao, C. S.; Rendina, A. R.; Schaeffer,

M. C.; Summerfield, J. D.; Swift, B. A.; Totoritis, R. D.; Ward, P.; Zhang, A.; Zhang, D.; Marquis, R. W.; Bertin, J.; Gough, P. J. DNA-encoded library screening identifies benzo[b][1,4]oxazepin-4-ones as highly potent and monoselective receptor interacting protein 1 kinase inhibitors. *J. Med. Chem.* **2016,** 59, 2163-2178.

25. Harris, P. A.; Berger, S. B.; Jeong, J. U.; Nagilla, R.; Bandyopadhyay, D.; Campobasso, N.; Capriotti, C. A.; Cox, J. A.; Dare, L.; Dong, X.; Eidam, P. M.; Finger, J. N.; Hoffman, S. J.; Kang, J.; Kasparcova, V.; King, B. W.; Lehr, R.; Lan, Y.; Leister, L. K.; Lich, J. D.; MacDonald, T. T.; Miller, N. A.; Ouellette, M. T.; Pao, C. S.; Rahman, A.; Reilly, M. A.; Rendina, A. R.; Rivera, E. J.; Schaeffer, M. C.; Sehon, C. A.; Singhaus, R. R.; Sun, H. H.; Swift, B. A.; Totoritis, R. D.; Vossenkamper, A.; Ward, P.; Wisnoski, D. D.; Zhang, D.; Marquis, R. W.; Gough, P. J.; Bertin, J. Discovery of a first-in-class receptor interacting protein 1 (RIP1) kinase specific clinical candidate (GSK2982772) for the treatment of inflammatory diseases. *J. Med. Chem.* **2017,** 60, 1247-1261.

26. Weisel, K.; Scott, N. E.; Tompson, D. J.; Votta, B. J.; Madhavan, S.; Povey, K.; Wolstenholme, A.; Simeoni, M.; Rudo, T.; Richards-Peterson, L.; Sahota, T.; Wang, J. G.; Lich, J.; Finger, J.; Verticelli, A.; Reilly, M.; Gough, P. J.; Harris, P. A.; Bertin, J.; Wang, M. L. Randomized clinical study of safety, pharmacokinetics, and pharmacodynamics of RIPK1 inhibitor GSK2982772 in healthy volunteers. *Pharmacol. Res. Perspect.* **2017,** 5, e00365.

27. Mullard, A. Microglia-targeted candidates push the Alzheimer drug envelope. *Nat. Rev. Drug Discov.* **2018,** 17, 303-305.

28. Cai, Z.; Liu, Z. G. Execution of RIPK3-regulated necrosis. *Mol. Cell Oncol.* **2014,** 1, e960759.

29. Moriwaki, K.; Chan, F. K. Necroptosis-independent signaling by the RIP kinases in inflammation. *Cell Mol. Life Sci.* **2016,** 73, 2325-2334.

30. Degterev, A.; Linkermann, A. Generation of small molecules to interfere with regulated necrosis. *Cell Mol. Life Sci.* **2016,** 73, 2251-2267.

31. Mandal, P.; Berger, S. B.; Pillay, S.; Moriwaki, K.; Huang, C.; Guo, H.; Lich, J. D.; Finger, J.; Kasparcova, V.; Votta, B.; Ouellette, M.; King, B. W.; Wisnoski, D.; Lakdawala, A. S.; DeMartino, M. P.; Casillas, L. N.; Haile, P. A.; Sehon, C. A.; Marquis, R. W.; Upton, J.; Daley-Bauer, L. P.; Roback, L.; Ramia,

N.; Dovey, C. M.; Carette, J. E.; Chan, F. K.; Bertin, J.; Gough, P. J.; Mocarski, E. S.; Kaiser, W. J. RIP3 induces apoptosis independent of pronecrotic kinase activity. *Mol. Cell* **2014,** 56, 481-495.

32. Newton, K.; Dugger, D. L.; Wickliffe, K. E.; Kapoor, N.; de Almagro, M. C.; Vucic, D.; Komuves, L.; Ferrando, R. E.; French, D. M.; Webster, J.; Roose-Girma, M.; Warming, S.; Dixit, V. M. Activity of protein kinase RIPK3 determines whether cells die by necroptosis or apoptosis. *Science* **2014,** 343, 1357-1360.

33. Li, J. X.; Feng, J. M.; Wang, Y.; Li, X. H.; Chen, X. X.; Su, Y.; Shen, Y. Y.; Chen, Y.; Xiong, B.; Yang, C. H.; Ding, J.; Miao, Z. H. The B-Raf(V600E) inhibitor dabrafenib selectively inhibits RIP3 and alleviates acetaminophen-induced liver injury. *Cell Death Dis.* **2014,** 5, e1278.

34. Flaherty, K. T.; Puzanov, I.; Kim, K. B.; Ribas, A.; McArthur, G. A.; Sosman, J. A.; O'Dwyer, P. J.; Lee, R. J.; Grippo, J. F.; Nolop, K.; Chapman, P. B. Inhibition of mutated, activated BRAF in metastatic melanoma. *N. Engl. J. Med.* **2010,** 363, 809-819.

35. Liao, D.; Sun, L.; Liu, W.; He, S.; Wang, X.; Lei, X. Necrosulfonamide inhibits necroptosis by selectively targeting the mixed lineage kinase domain-like protein. *MedChemCommun* **2014,** 5, 333-337.

36. Chen, X.; Zhuang, C.; Ren, Y.; Zhang, H.; Qin, X.; Hu, L.; Fu, J.; Miao, Z.; Chai, Y.; Liu, Z. G.; Zhang, H.; Cai, Z.; Wang, H. Y. Identification of TAK-632 and its analogues as potent inhibitors of necroptosis by targeting RIPK1 and RIPK3. *Br. J. Pharmacol.* [Online early access]. DOI: 10.1111/bph.14653. Published Online: Mar 1, 2019. https://bpspubs.onlinelibrary.wiley.com/doi/10.1111/bph.14653 (Mar 1, 2019).

37. Okaniwa, M.; Hirose, M.; Arita, T.; Yabuki, M.; Nakamura, A.; Takagi, T.; Kawamoto, T.; Uchiyama, N.; Sumita, A.; Tsutsumi, S.; Tottori, T.; Inui, Y.; Sang, B. C.; Yano, J.; Aertgeerts, K.; Yoshida, S.; Ishikawa, T. Discovery of a selective kinase inhibitor (TAK-632) targeting pan-RAF inhibition: design, synthesis, and biological evaluation of C-7-substituted 1,3-benzothiazole derivatives. *J. Med. Chem.* **2013,** 56, 6478-6494.

38. Nakamura, A.; Arita, T.; Tsuchiya, S.; Donelan, J.; Chouitar, J.; Carideo, E.; Galvin, K.; Okaniwa, M.; Ishikawa, T.; Yoshida, S. Antitumor activity of the selective pan-RAF inhibitor TAK-632 in BRAF inhibitor-resistant melanoma. *Cancer Res.* **2013,** 73, 7043-7055.

39. Najjar, M.; Suebsuwong, C.; Ray, S. S.; Thapa, R. J.; Maki, J. L.; Nogusa, S.; Shah, S.; Saleh, D.; Gough, P. J.; Bertin, J.; Yuan, J.; Balachandran, S.; Cuny, G. D.; Degterev, A. Structure guided design of potent and selective ponatinib-based hybrid inhibitors for RIPK1. *Cell Rep.* **2015,** 10, 1850-1860.

40. Fauster, A.; Rebsamen, M.; Huber, K. V.; Bigenzahn, J. W.; Stukalov, A.; Lardeau, C. H.; Scorzoni, S.; Bruckner, M.; Gridling, M.; Parapatics, K.; Colinge, J.; Bennett, K. L.; Kubicek, S.; Krautwald, S.; Linkermann, A.; Superti-Furga, G. A cellular screen identifies ponatinib and pazopanib as inhibitors of necroptosis. *Cell Death Dis.* **2015,** 6, e1767.

41. Martens, S.; Jeong, M.; Tonnus, W.; Feldmann, F.; Hofmans, S.; Goossens, V.; Takahashi, N.; Brasen, J. H.; Lee, E. W.; Van der Veken, P.; Joossens, J.; Augustyns, K.; Fulda, S.; Linkermann, A.; Song, J.; Vandenabeele, P. Sorafenib tosylate inhibits directly necrosome complex formation and protects in mouse models of inflammation and tissue injury. *Cell Death Dis.* **2017,** 8, e2904.

42. Xie, T.; Peng, W.; Yan, C.; Wu, J.; Gong, X.; Shi, Y. Structural insights into RIP3-mediated necroptotic signaling. *Cell Rep.* **2013,** 5, 70-78.

43. Wang, W.; Marinis, J. M.; Beal, A. M.; Savadkar, S.; Wu, Y.; Khan, M.; Taunk, P. S.; Wu, N.; Su, W.; Wu, J.; Ahsan, A.; Kurz, E.; Chen, T.; Yaboh, I.; Li, F.; Gutierrez, J.; Diskin, B.; Hundeyin, M.; Reilly, M.; Lich, J. D.; Harris, P. A.; Mahajan, M. K.; Thorpe, J. H.; Nassau, P.; Mosley, J. E.; Leinwand, J.; Kochen Rossi, J. A.; Mishra, A.; Aykut, B.; Glacken, M.; Ochi, A.; Verma, N.; Kim, J. I.; Vasudevaraja, V.; Adeegbe, D.; Almonte, C.; Bagdatlioglu, E.; Cohen, D. J.; Wong, K. K.; Bertin, J.; Miller, G. RIP1 kinase drives macrophage-mediated adaptive immune tolerance in pancreatic cancer. *Cancer Cell* **2018,** 34, 757-774 e757.

44. Xin, J.; You, D.; Breslin, P.; Li, J.; Zhang, J.; Wei, W.; Cannova, J.; Volk, A.; Gutierrez, R.; Xiao, Y.; Ni, A.; Ng, G.; Schmidt, R.; Xia, Z.; Pan, J.; Chen, H.; Patel, M. M.; Kuo, P. C.; Nand, S.; Kini, A. R.; Zhang, J.; Chen, J.; Zhu, J.; Zhang, J. Sensitizing acute myeloid leukemia cells to induced differentiation by inhibiting the RIP1/RIP3 pathway. *Leukemia* **2017,** 31, 1154-1165.

45. Wang, H.; Wei, W.; Lan, X.; Liu, N.; Li, Y.; Ma, H.; Sun, T.; Peng, X.; Zhuang, C.; Yu, J. Neuroprotective effect of swertiamain on cerebral ischemia/reperfusion injury by inducing the Nrf2 protective

pathway. *ACS Chem. Neurosci.* [Online early access]. DOI: 10.1021/acschemneuro.8b00605. Published Online: Feb 19, 2019. https://pubs.acs.org.ccindex.cn/doi/10.1021/acschemneuro.8b00605 (Feb 19, 2019).

46. Zhuang, C.; Narayanapillai, S.; Zhang, W.; Sham, Y. Y.; Xing, C. Rapid identification of Keap1-Nrf2 small-molecule inhibitors through structure-based virtual screening and hit-based substructure search. *J. Med. Chem.* **2014,** 57, 1121-1126.

Table of Contents graphic

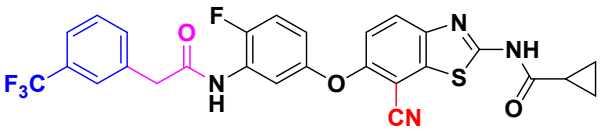

6 (TAK-632)

HT-29, anti-necroptosis, EC_{50} = 1.44 ± 0.62 μM
Cytotoxicity IC_{50} > 50 μM
RIPK1 K_d = 480 nM
RIPK3 K_d = 105 nM
In vivo protection of SIRS: 70% at 100 mg/kg
20% at 25 mg/kg

Optimization

SAR

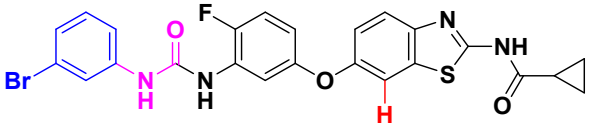

42

HT-29, anti-necroptosis, EC_{50} = 0.44 ± 0.10 μM
Cytotoxicity IC_{50} > 50 μM
RIPK1 K_d > 5000 nM
RIPK3 K_d = 81 nM
In vivo protection of SIRS: 100% at 25 mg/kg
90% at 5 mg/kg
Oral bioavailability (F) = 25.2%